frontiers | Frontiers in Earth Science

TYPE Original Research
PUBLISHED 28 September 2023
DOI 10.3389/feart.2023.1213958



OPEN ACCESS

EDITED BY
J. Gregory Shellnutt,
National Taiwan Normal University, Taiwan

REVIEWED BY
K. R. Hari,
Pandit Ravishankar Shukla University, India
Thuy Thanh Pham,
National Taiwan University, Taiwan

*CORRESPONDENCE
Yu-Ling Lin,
lulumilin@ntnu.edu.tw
Tung-Yi Lee,
t44001@ntnu.edu.tw

RECEIVED 28 April 2023
ACCEPTED 21 August 2023
PUBLISHED 28 September 2023

CITATION
Lin Y-L, Lee T-Y, Lee H-Y, Iizuka Y, Quek LX and Charusiri P (2023), Zircon U-Pb geochronology of the Lan Sang gneisses and its tectonic implications for the Mae Ping shear zone, NW Thailand. *Front. Earth Sci.* 11:1213958. doi: 10.3389/feart.2023.1213958



# Zircon U-Pb geochronology of the Lan Sang gneisses and its tectonic implications for the Mae Ping shear zone, NW Thailand

Yu-Ling Lin[1]*, Tung-Yi Lee[1]*, Hao-Yang Lee[2], Yoshiyuki Iizuka[2], Long Xiang Quek[3] and Punya Charusiri[4]

[1]Department of Earth Sciences, National Taiwan Normal University, Taipei, Taiwan, [2]Institute of Earth Sciences, Academia Sinica, Taipei, Taiwan, [3]Key Laboratory of Computational Geodynamics, College of Earth and Planetary Sciences, College of Earth and Planetary Sciences, University of Chinese Academy of Sciences, Beijing, China, [4]Department of Geology, Faculty of Science, Chulalongkorn University, Bangkok, Thailand

The Mae Ping shear zone (MPSZ), a major shear zone trending NW-SE in Thailand, is responsible for the left-lateral displacement of the N-S Triassic-Jurassic granitoid and gneiss belt. This displacement is postulated to have contributed to Cenozoic extrusion tectonics. Within the Lan Sang National Park, the MPSZ exposes several intensely deformed lithologies, collectively known as the Lan Sang gneisses. These gneisses have attracted considerable attention for their potential to substantiate the extrusion model. However, the timing of the emplacement of the orthogneiss protolith is still debated. Moreover, the origin and distribution of the Eocene syn-shearing granodiorite within this shear zone are not well understood. To shed light on the magmatic history of the MPSZ, this study utilized zircon U-Pb geochronology to systematically investigate the Lan Sang gneisses. Our findings demonstrate that these gneisses can be categorized into paragneiss and orthogneiss groups. Paragneiss samples feature zircons displaying rounded detrital cores ranging from 3,078 to 450 Ma, with metamorphic rim overgrowth of ca. 200 Ma (most Th/U <0.01). This indicates that their Paleozoic sedimentary protoliths experienced high-grade metamorphism during the Triassic-Jurassic Indosinian orogeny. On the other hand, zircon from orthogneiss samples shows that their magmatic protoliths were predominantly emplaced either around ~200 Ma or within 45-32 Ma. The Eocene-Oligocene magmatism likely coincided with the proposed Eocene metamorphism. Since these samples were deformed by left-lateral shearing, the left-lateral motion of the MPSZ probably ended after 32 Ma. Eocene-Oligocene magmatic events have also been identified in granite, mylonite, and gneiss samples from other regions along the Sibumasu terrane, including the Three Pagodas, Klaeng, Ranong, Khlong Marui shear zones, and the Doi Inthanon area. The Eocene-Oligocene magmatism was likely linked with the movement of the shear zones and may be responsible for the regional cooling pattern. The spatial and temporal distribution of the Eocene-Oligocene magmatism within the Sibumasu terrane supports the hypothesis that the inward migration of magmatism in the overriding plate resulted from the shallowing of the Neo-Tethyan slab.

KEYWORDS

**Lan Sang gneisses, Mae Ping shear zone, zircon U-Pb geochronology, Sibumasu, Thailand, syn-shearing intrusion**

# 1 Introduction

Numerous studies have focused on the Cenozoic extrusion tectonics induced by the India-Eurasia collision (as shown in Figure 1), with the aim of determining the timing of major shear zones by dating the associated magmatism or metamorphism (Scharer et al., 1994; Wang et al., 1998; Zhang and Schärer, 1999; Searle, 2006; Liang et al., 2007; Chung et al., 2008; Watkinson et al., 2011; Nantasin et al., 2012; Kanjanapayont et al., 2013; Palin et al., 2013; Tang et al., 2013; Liu et al., 2015; Österle et al., 2019; Li et al., 2021). These shear zones include the Ailao Shan-Red River shear zone (AS-RRSZ), the Mae Ping shear zone (MPSZ, also known as the Wang Chao fault zone), the Three Pagodas shear zone (TPSZ), the Klaeng shear zone (KSZ), the Ranong shear zone (RSZ), and the Khlong Marui shear zone (KSZ). It is believed that these shear zones were motivated by the indentation of India into Asia and have accommodated notable deformation. In particular, the MPSZ is thought to have played a crucial role in facilitating the southeastward extrusion of Indochina through its movement (Tapponnier et al., 1982; Peltzer and Tapponnier, 1988; Lacassin et al., 1997).

Previous studies have applied various geochronological methods to the MPSZ and its surrounding area to elucidate its evolution (Ahrendt et al., 1993; Lacassin et al., 1997; Morley et al., 2007; Palin et al., 2013; Österle et al., 2019; Lin et al., 2021). Mineral cooling ages have been obtained to discern the timing of rapid cooling or exhumation potentially linked to the motion of the MPSZ (Ahrendt et al., 1993; Lacassin et al., 1997; Morley et al., 2007; Lin et al., 2021). The rapid cooling during 42-30 Ma was attributed to the left-lateral shearing of the MPSZ, followed by the subsequent cooling between 23 and 18 Ma, probably due to the reversal of right-lateral movement. However, the regional cooling pattern indicates that the strike-slip deformation of the MPSZ did not dominate the cooling history. The exposure of the Lan Sang gneisses is more associated with regional exhumation patterns than the uplift and erosion caused by shearing (Morley et al., 2007). Consequently, Palin et al. (2013) and Österle et al. (2019) endeavored to study metamorphism and magmatism in an effort to achieve a more comprehensive understanding of the MPSZ.

Palin et al. (2013) proposed that the protolith of the Lan Sang orthogneiss was emplaced during the Early Cretaceous based on monazite Th-Pb dates. It was subsequently subjected to an Eocene prograde metamorphism during 45-37 Ma, prior to the ductile shearing of the MPSZ. They concluded that neither metamorphism nor regional cooling was directly related to the shearing of MPSZ. The zircon U-Pb geochronology of Österle et al. (2019) revealed the granitic protolith of an augen gneiss intruded metasedimentary basement during the Late Triassic. They suggested the Eocene metamorphism commenced by ~45 Ma and subsequently led to partial melting of basement gneisses. This metamorphism culminated in the intrusion of granodiorite around 35 Ma, accompanied by contemporaneous ductile shearing along the MPSZ. Their findings are very encouraging since previous zircon U-Pb studies only indicated a Triassic-Jurassic amphibolite facies metamorphism (Ahrendt et al., 1993; Kanjanapayont et al., 2011).

However, further investigation remains essential to ascertain the emplacement timing of the protolith of the Lan Sang orthogneiss and whether it occurred during the Early Cretaceous or the Late Triassic. In fact, not only shearing but also magmatism can contribute to metamorphism or mineral cooling. Therefore, a detailed examination of the interrelationships between the Eocene metamorphism, granodioritic intrusion, regional cooling, and

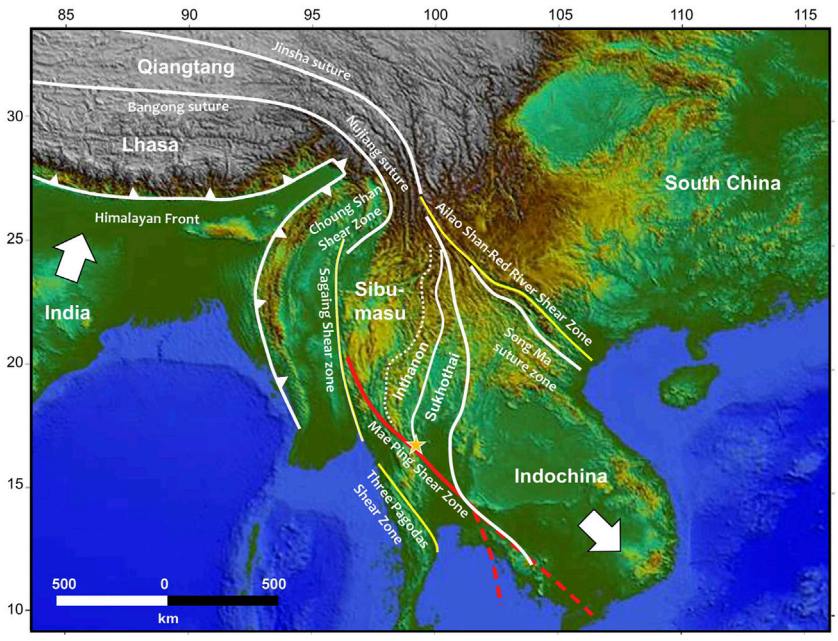


FIGURE 1
DTM map of SE Asia showing the extrusion tectonics based on Leloup et al. (1995), Ueno and Hisada (2001), and Sone et al. (2012). The orange star marks the position of the Lan Sang gneisses within the MPSZ. The left-lateral motion of the MPSZ is thought to have facilitated the extrusion of Indochina.

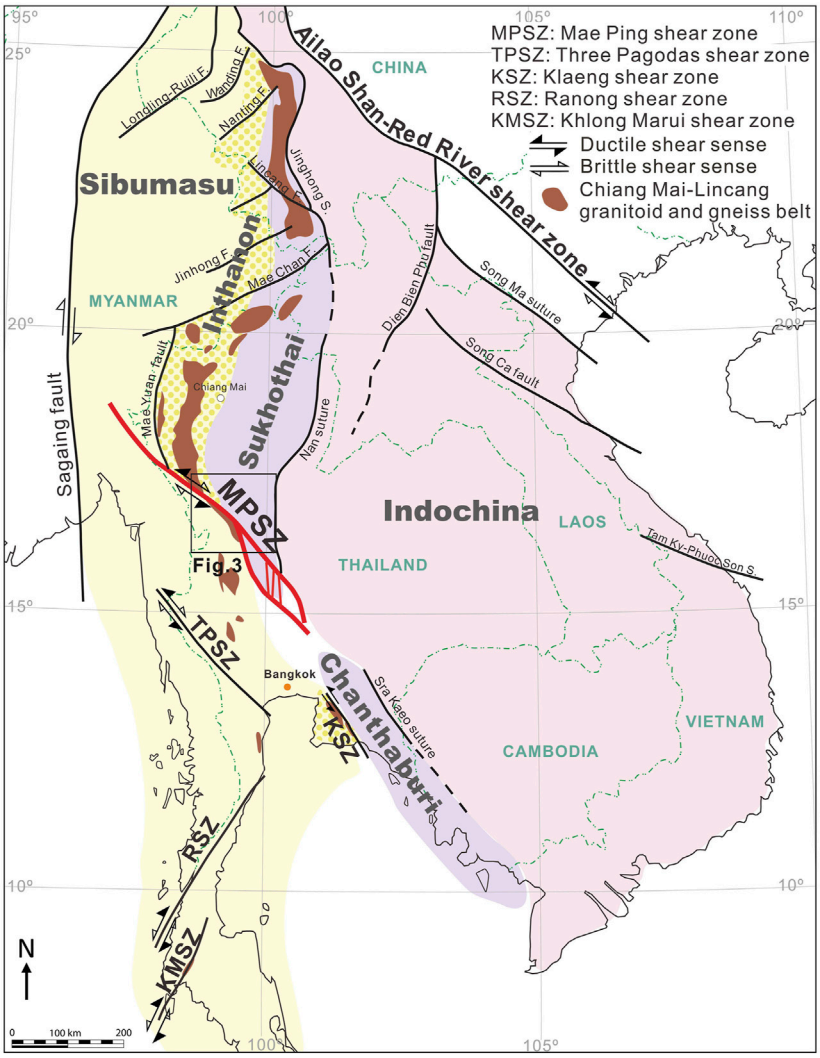


FIGURE 2
Tectonic subdivision map of SE Asia (after Lacassin et al., 1997; Sone et al., 2012; Deng et al., 2014). The MPSZ stretches from the Sibumasu terrane, displacing the Inthanon zone and the Sukhothai arc; however, its southeastward extension is still uncertain.

shearing is necessary for a comprehensive tectonic reconstruction of the MPSZ. In this study, we present new zircon U-Pb geochronology data on the Lan Sang gneisses, aiming to: 1) provide detailed age constraints to elucidate the complex thermal history; 2) offer insights into the spatial and temporal distribution of Eocene magmatism; 3) explore the correlations between magmatism, metamorphism, and shear activity; and 4) propose a tectonic reconstruction of the MPSZ.

## 2 Geological background

The NW-SE trending MPSZ stretches for approximately 500 km, extending from the Sagaing fault in Myanmar to northern Thailand. However, uncertainties persist about its continuation to the southeast (Morley et al., 2007). It is inferred that the MPSZ has undergone left-lateral deformation for at least 150 km (Lacassin et al., 1997) and possibly up to 300 km (Peltzer and Tapponnier, 1988). Similar to the AR-RRSZ, the MPSZ may also have experienced a later reversal to right-lateral strike-slip motion since the Oligocene or during the Miocene (Polachan et al., 1991; Lacassin et al., 1997). In addition to these uncertainties, the tectonic framework of the MPSZ is complex.

Southeast Asia comprises heterogeneous continental fragments derived from the Gondwana margin and assembled by the closure of Paleo-, Meso-, and Neo-Tethys oceans and back-arc basins (Metcalfe, 2013). In particular, the MPSZ occupies an important position as it encompasses the major tectonic fragments of Southeast Asia, such as the Sibumasu terrane, the Inthanon accretionary zone, the Sukhothai island arc, and the Indochina terrane (Figure 2; Metcalfe, 2011; Sone et al., 2012). The Sibumasu terrane consists of Phanerozoic rocks and a Cambrian-Ordovician crystalline basement that probably formed in a magmatic arc-related regime on the Gondwana India-Australia margin around 502-477 Ma (Lin et al., 2013; Kawakami et al., 2014; Dew et al., 2018). The Indochina terrane is thought to comprise several micro-terranes. Magmatic

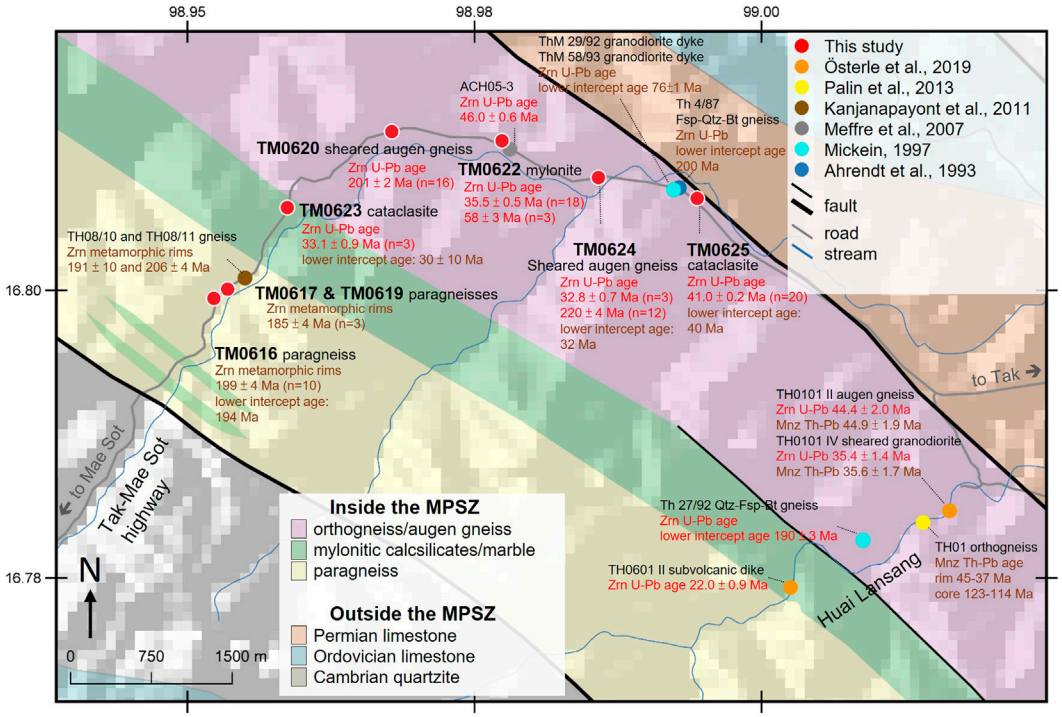


FIGURE 3
Sample location map showing the thermal history of the Lan Sang gneisses by highlighting zircon U-Pb and monazite Th-Pb ages. The simplified geological map (modified from Lacassin et al., 1997; DMR, 1999; Österle et al., 2019) is overlaid with SRTM 90 m DEM data (Jarvis et al., 2008).

and detrital zircon dates indicate that the Indochina terrane underwent two major magmatic events at 480-404 Ma and 300-230 Ma (Khin et al., 2014; Arboit et al., 2016; Wang et al., 2016; Kawaguchi et al., 2021). The Sukhothai arc developed along the margin of Indochina as a result of the Paleo-Tethys ocean subducting beneath Indochina and consists primarily of I-type granitoids of 238-228 Ma (zircon U-Pb ages, Khin et al., 2014; Dew et al., 2018). The Inthanon zone represents a remnant of the Paleo-Tethys accretionary complex that overlies the Sibumasu terrane (Sone et al., 2012).

In addition to the tectonic fragments, the MPSZ has left-laterally displaced the N-S Triassic-Jurassic granitoid and gneiss belt, known as the Chiang Mai-Lincang belt (CM-LB, Figure 2). Therefore, the MPSZ may incorporate magmatic or metamorphic ages originating from the CM-LB. In NW Thailand, the formation of the CM-LB resulted from the collision between the Sibumasu and Indochina terranes, an event commonly referred to as the Indosinian orogeny, following the closure of the Paleo-Tethys (Searle et al., 2012; Palin et al., 2013). This granitoid and gneiss belt has attracted considerable attention because of its tin and tungsten mineralization (Searle et al., 2012). According to the studies of the Doi Inthanon and Doi Suthep areas, this belt should have experienced magmatism and high-grade metamorphism at 221-210 Ma, then upper-amphibolite facies metamorphism at 84-67 Ma, and a late tectonothermal event at 34-24 Ma (Dunning et al., 1995; Macdonald et al., 2010; Gardiner et al., 2016). The MPSZ may contain similar ages.

Due to intense weathering and dense vegetation, only a few suitable outcrops are available to investigate the MPSZ. Within the Lan Sang National Park, the Tak-Mae Sot highway traverses the 5 km-wide MPSZ and exposes outcrops of deformed high-grade paragneiss, orthogneiss, mylonite, cataclasite, calc-silicate, leucogranite, and minor undeformed intrusive rocks (Figure 3). These high-grade and intensely deformed rocks are collectively referred to as the Lan Sang gneisses. In addition to the highway, samples were also collected from Huai Lansang, a stream located ~6 km away from it (Mickein, 1997; Palin et al., 2013; Österle et al., 2019). The exposure of Lan Sang gneisses along these two transects has contributed valuable insights into the tectonic evolution of the MPSZ, although a detailed U-Pb dating study is still lacking.

## 3 Previous geochronologic constraints for the MPSZ

Zircon U-Pb dating of a feldspar-quartz-biotite gneiss revealed an inherited core age of 1,530 Ma and a discordia lower intercept age of around 200 Ma based on six zircon grains, indicating a Triassic amphibolite facies metamorphism. While biotite yielded K/Ar cooling ages of 32-30 Ma, this may be due to the strong uplift caused by shearing along the MPSZ (Ahrendt et al., 1993). Biotite and K-feldspar $^{40}Ar/^{39}Ar$ ages of Lan Sang gneisses indicated rapid cooling at 30.5 and 23 Ma, which were interpreted as the termination of left-lateral shear and the onset of right-lateral motion due to E-W extension, respectively (Lacassin et al., 1997). Zircon fission track ages of 36-28 Ma indicate exhumation due to the regional uplift, while apatite fission track ages of 25-19 Ma may follow the Late Oligocene-Early Miocene extension (Morley et al., 2007).

**TABLE 1 Sample descriptions.**

| Sample | Lithology | GPS coordinates | | Mineral assemblage | Major foliation Dip/Dip Az |
|---|---|---|---|---|---|
| *Paragneiss samples* | | | | | |
| TM0616 | Paragneiss | N16.7993 | E98.9523 | Qz+Pl+Kfs+Ms | 62/061 |
| TM0617 | Paragneiss | N16.8001 | E98.9535 | Qz+Pl+Kfs+Ms | 79/051 |
| TM0619 | Paragneiss | N16.8001 | E98.9535 | Qz+Pl+Kfs+Bt+Hb | 70/061 |
| *Orthogneiss samples* | | | | | |
| TM0623 | Cataclasite | N16.8072 | E98.9587 | Qz+Pl+Kfs+Bt | 34/024 |
| TM0620 | Sheared augen gneiss | N16.8138 | E98.9678 | Qz+Pl+Kfs+Bt | 52/059 |
| TM0622 | Mylonite | N16.813 | E98.9774 | Qz+Pl+Kfs+Bt | 50/067 |
| TM0624B | Sheared augen gneiss | N16.8098 | E98.9858 | Biotite rich layer: Qz+Pl+Kfs+Bt+Hb | 46/058 |
| | | | | Feldspathic layer: Qz+Pl+Kfs+Bt | |
| TM0625 | Cataclasite | N16.8080 | E98.9944 | Qz+Pl+Kfs+Bt+Ms | 41/042 |

Metamorphic zircon rims of two Lan Sang gneisses overgrew around 191 ± 10 and 206 ± 4 Ma (Kanjanapayont et al., 2011), suggesting Triassic-Jurassic metamorphism. Monazite U-Th-Pb geochronology on the Lan Sang orthogneiss indicated that its magmatic protolith was likely emplaced at 123-114 Ma, with subsequent metamorphism occurring at 45-37 Ma (Palin et al., 2013). Zircon U-Pb dating suggested the protolith of augen gneiss may have intruded into the metasedimentary rocks at ~235–220 Ma (Österle et al., 2019). Zircons in this augen gneiss exhibit a second age cluster at 45 Ma, whereas zircons in the sheared granodiorite display a dominant age cluster at 35 Ma. Österle et al. (2019) interpreted these findings to indicate that metamorphism likely began around 45 Ma and reached a climax with partial melting and the intrusion of granodiorite at 35 Ma. $^{40}Ar/^{39}Ar$ thermochronology on the leucogranite within the MPSZ, along with careful deformation temperature estimation, suggested that left-lateral shear occurred at least from 42 to 30 Ma (Lin et al., 2021).

# 4 Methods

## 4.1 Sampling

Paragneiss, mylonite, cataclasite, and sheared augen gneiss samples were collected from outcrops along the highway in the Lan Sang National Park (Table 1). Samples were collected at intervals of at least every 1 km. The orientation of the major foliation plane in each sample was also measured in the field. Photographs of the outcrops can be found in Figure 3 by Lin et al. (2021). Paragneiss samples were named according to the sedimentary characteristics revealed by zircon U-Pb dating. The nomenclature of other samples is based on their textures from hand specimens, as they were all deformed (Figure 4). In the accompanying text, figures, and tables, samples are arranged according to their geographical locations, from west to east. This is intended to facilitate understanding and comparison of the results. Thin sections of these samples were examined to observe the deformation textures (Figure 5) in order to infer deformation conditions and timing related to the magmatism. Mineral abbreviations in Figure 5 and Table 1 follow Whitney and Evans (2010).

## 4.2 Zircon U-Pb dating

Zircons were separated from 1-2 kg of samples using magnetic and heavy liquid separation techniques. For each sample, approximately 100–120 zircon grains were mounted, filling the epoxy resin to a depth of ~1 cm. After 24 h of solidification, the mold and the tape were removed from the epoxy discs. The discs were ground using a Struers MD-Piano 500 (Struers, Copenhagen, Denmark) resin-bonded diamond disc until a suitable zircon cross-section was exposed, followed by polishing with 3 μm diamond suspensions. Cathodoluminescence (CL) electron images of zircon grains were taken using a JEOL (Japan Electron Optics Laboratory Co., Ltd.) JSM-6360LV scanning electron microscope (SEM) at the Institute of Earth Sciences, Academia Sinica, Taiwan. These images were used to examine the crystal shapes and internal zoning structures and to select suitable positions for U-Pb isotope analyses.

Zircon U-Pb dating was conducted using an Agilent 7500s quadrupole inductively coupled plasma mass spectrometer (ICP-MS) (Agilent Technologies, Inc., Santa Clara, United States) equipped with a New Wave UP-213 laser ablation system (Electro Scientific Industries, Inc., Portland, United States) at the National Taiwan University (NTU), Taipei, Taiwan. The laser beam was set to a diameter of 35 μm, with a repetition rate of 4 Hz and an energy of 10 J/cm$^2$. For instrumental drift correction, the GJ-1 zircon served as the primary standard, while the Harvard reference zircon 91,500 and the Australian Mud Tank carbonatite zircon MT were employed as secondary standards for measurement quality monitoring. Analytical procedures and operating conditions followed those outlined in Chiu et al. (2009). The upper and lower intercepts, concordia ages, and plots were calculated and generated using the Excel add-in of the Isoplot 4.15 software (Ludwig, 2008). Of the 366 analyses that underwent common lead correction, 361 of them showed age uncertainty ≤3% at the 1σ level. Age discordance was calculated based on the relative age

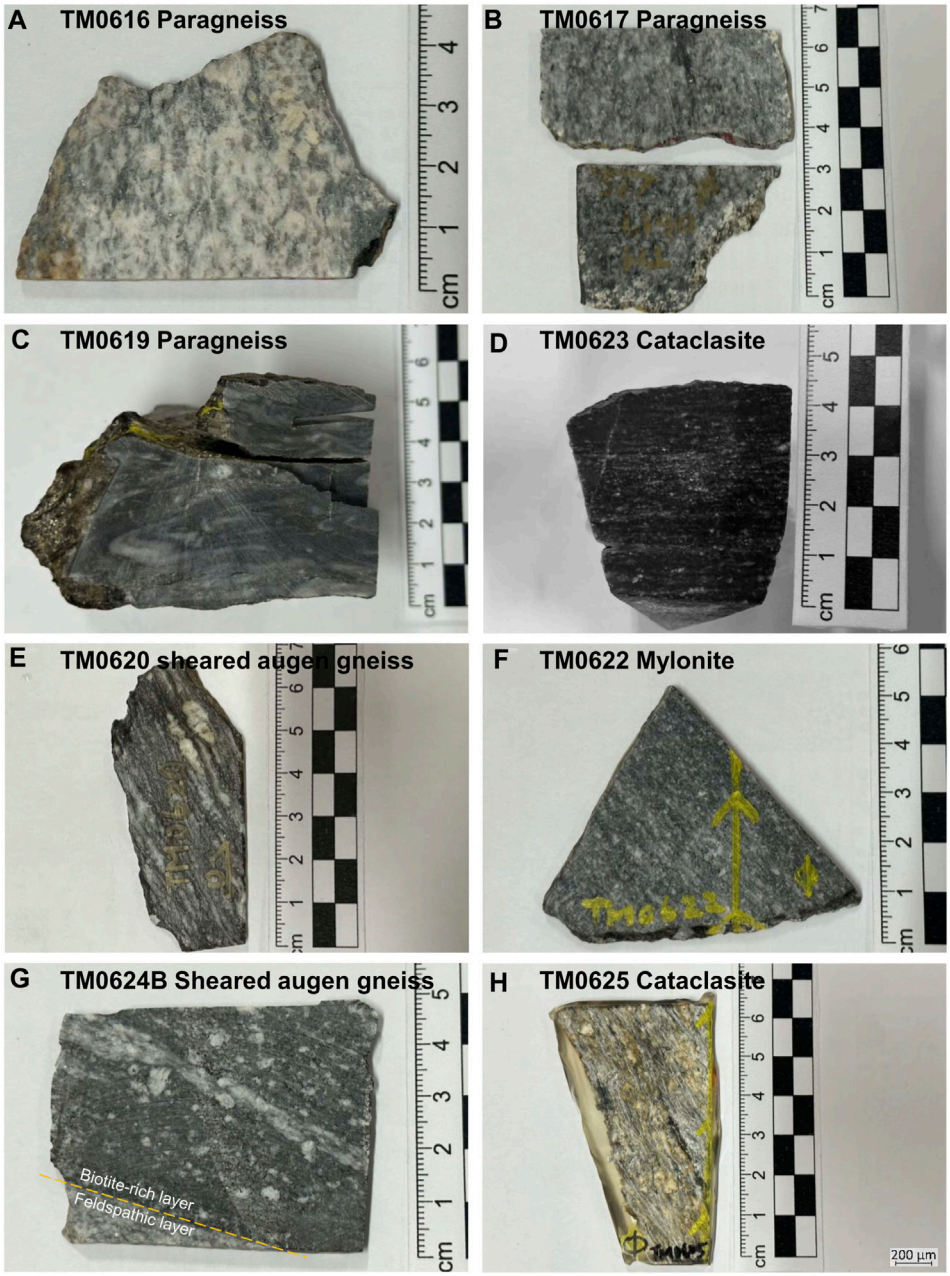


FIGURE 4
Representative photographs of hand specimens taken from samples of the Lan Sang gneisses. **(A–C)** paragneiss samples. **(D–H)** orthogneiss samples.

difference between the $^{207}Pb/^{235}U$ and $^{206}Pb/^{238}U$ ages (for $^{206}Pb/^{238}U$ ages <1,000 Ma) or between the $^{206}Pb/^{238}U$ and $^{207}Pb/^{206}Pb$ ages (for $^{206}Pb/^{238}U$ ages >1,000 Ma). Age spectra for data within 30% discordance were generated using the "detzrcr" software package developed in R (Andersen et al., 2018).

# 5 Results

All samples exhibit a sheared fabric indicating left-lateral shear sense. The major foliation planes measured at sample locations all dip towards the NE (Table 1), consistent with the findings reported by Lacassin et al. (1997). The paragneiss samples generally have steeper major foliation planes compared to the orthogneiss samples.

## 5.1 TM0616 feldspathic paragneiss

TM0616 is a muscovite feldspathic paragneiss (Figure 5A). Quartz shows dynamic recrystallization of bulging (BLG), subgrain rotation (SGR), and grain boundary migration (GBM). Sericite is observed both surrounding and embedded within the deformed plagioclase

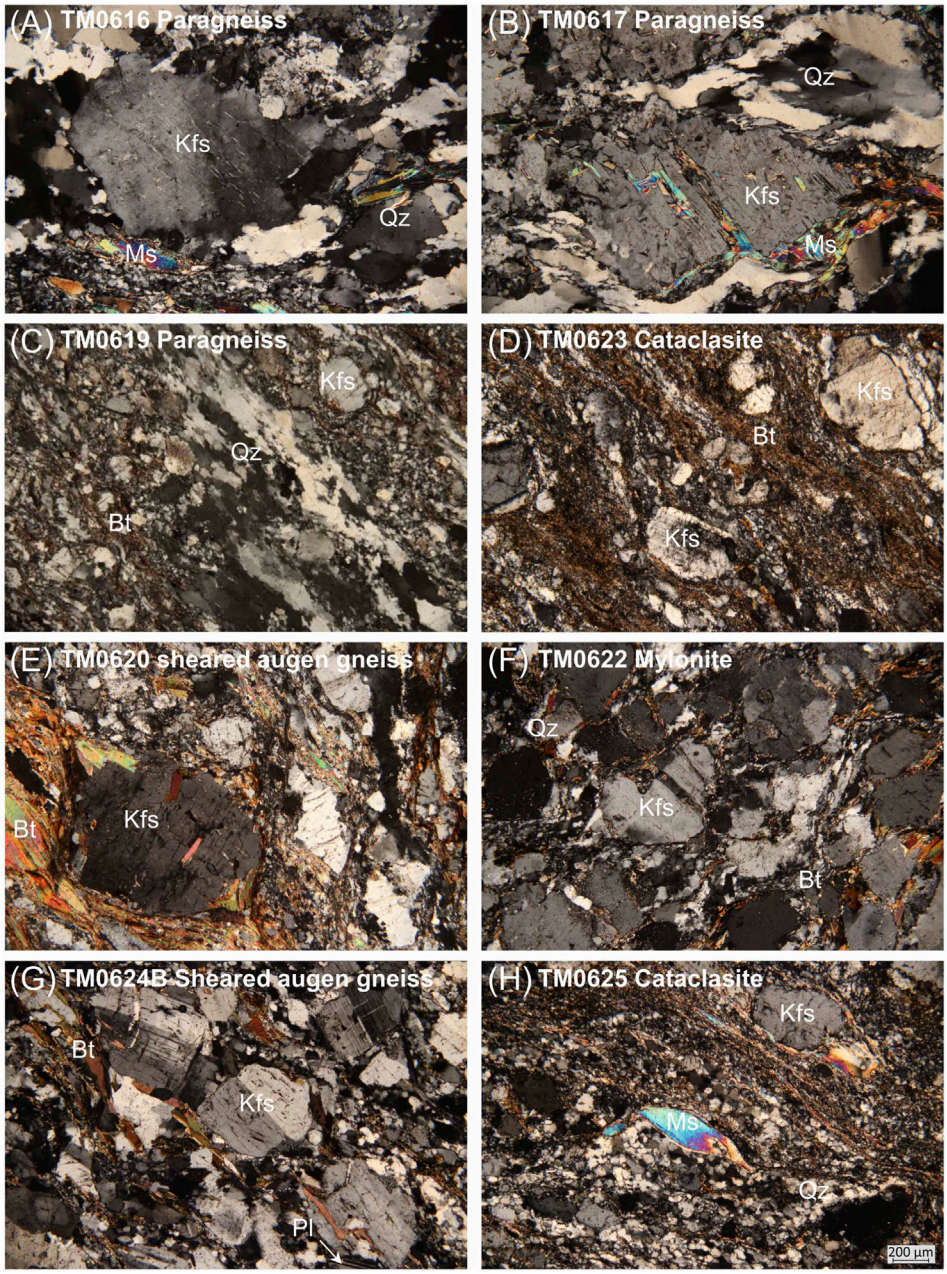


FIGURE 5
Representative photomicrographs of thin sections taken from samples of the Lan Sang gneisses. **(A–C)** paragneiss samples. **(D–H)** orthogneiss samples. All images were viewed under crossed polars at the same magnification. Undulose extinction and grain size reduction in feldspar, quartz, and mica indicate these rocks should have experienced plastic to brittle deformation. Mineral abbreviations follow Whitney and Evans (2010).

porphyroclast, pointing to the alteration of plagioclase through the Na-K exchange reaction. Plagioclase porphyroclasts show deformation twinning. The microstructure of quartz and plagioclase indicates that the deformation temperature could be as high as 600°C (Stipp et al., 2002; Passchier and Trouw, 2005). Fish-shaped muscovite was mainly deformed by grain size reduction.

Zircon grains from TM0616 display short prismatic shapes with lengths of ~200 μm. SEM-CL images reveal that most of the zircons are sub-euhedral and exhibit distinct core-rim structures. The cores are characterized by rounded shapes with bright oscillatory zoning, while the rims appear dull and cloudy without clear zonation (Figure 6). A total of 32 analyses were conducted on this sample, resulting in ages ranging from 2,511 to 191 Ma with a concordia age of 199 ± 4 Ma (Table 2; Figure 7A). Within these analyses, 18 zircon cores yielded ages of 2,511-462 Ma, with an average Th/U ratio of 0.46 (Figures 8A, 9). On the other hand, 14 zircon rim analyses yielded ages of 449, 249, 227, and 202-191 Ma. These rim analyses mostly fell on the concordia curve, although a few of them derived a lower intercept age of 194 ± 8 Ma (Figure 7A). A concordia age of 199 ± 4 Ma was calculated from these rim analyses, which showed an average Th/U ratio of 0.024.

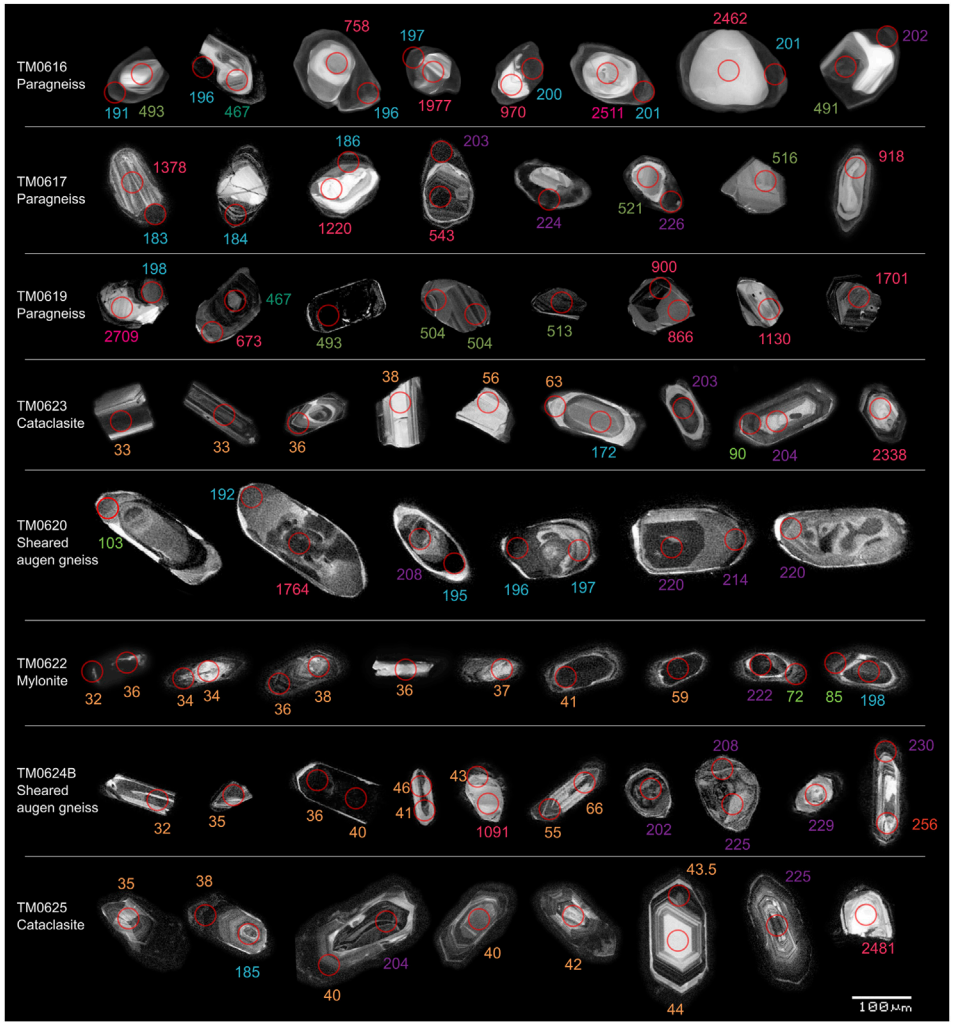


FIGURE 6
Representative zircon SEM cathodoluminescence images. Red circles mark the positions of U-Pb analyses. Ages have been common-lead corrected.

**TABLE 2 Summary of zircon U-Pb geochronology data.**

| Sample | Lithology | Age range (Ma) | | Concordia age | | | | Lower intercept age | Age clusters |
|---|---|---|---|---|---|---|---|---|---|
| | | min | max | (Ma) | n | MSWD | Th/U | (Ma) | (Ma) |
| TM0616 | Paragneiss | 191 ± 4 | 2,511 ± 24 | 199 ± 4 | 10 | 16 | 0.024 | 194 ± 8 | 198, 468 |
| TM0617 | Paragneiss | 179 ± 4 | 2,747 ± 14 | 185 ± 4 | 3 | 1.8 | 0.004 | | 184, 225, 514, 915 |
| TM0619 | Paragneiss | 198 ± 5 | 3,078 ± 14 | | | | | | 504, 726, 886, 986 |
| TM0623 | Cataclasite | 32.6 ± 0.8 | 2,438 ± 17 | 33.1 ± 0.9 | 3 | 3.5 | 0.59 | 30 ± 10 | 34 |
| TM0620 | Sheared augen gneiss | 103 ± 2 | 1764 ± 23 | 201 ± 2 | 16 | 0.24 | 0.37 | | 194, 208, 214 |
| TM0622 | Mylonite | 31.6 ± 0.6 | 924 ± 17 | 35.5 ± 0.5 | 18 | 0.073 | 0.62 | | 36, 200 |
| | | | | 58 ± 3 | 3 | 7.8 | 0.23 | | |
| TM0624B | Sheared augen gneiss | 32.4 ± 0.6 | 2,471 ± 17 | 32.8 ± 0.7 | 3 | 4.8 | 1.11 | 32 ± 6 | 33, 41, 211, 219 |
| | | | | 220 ± 4 | 12 | 0.079 | 0.57 | | |
| TM0625 | Cataclasite | 34.7 ± 0.9 | 2,481 ± 22 | 41.0 ± 0.2 | 20 | 3.7 | 0.27 | 40 ± 2 | 41 |

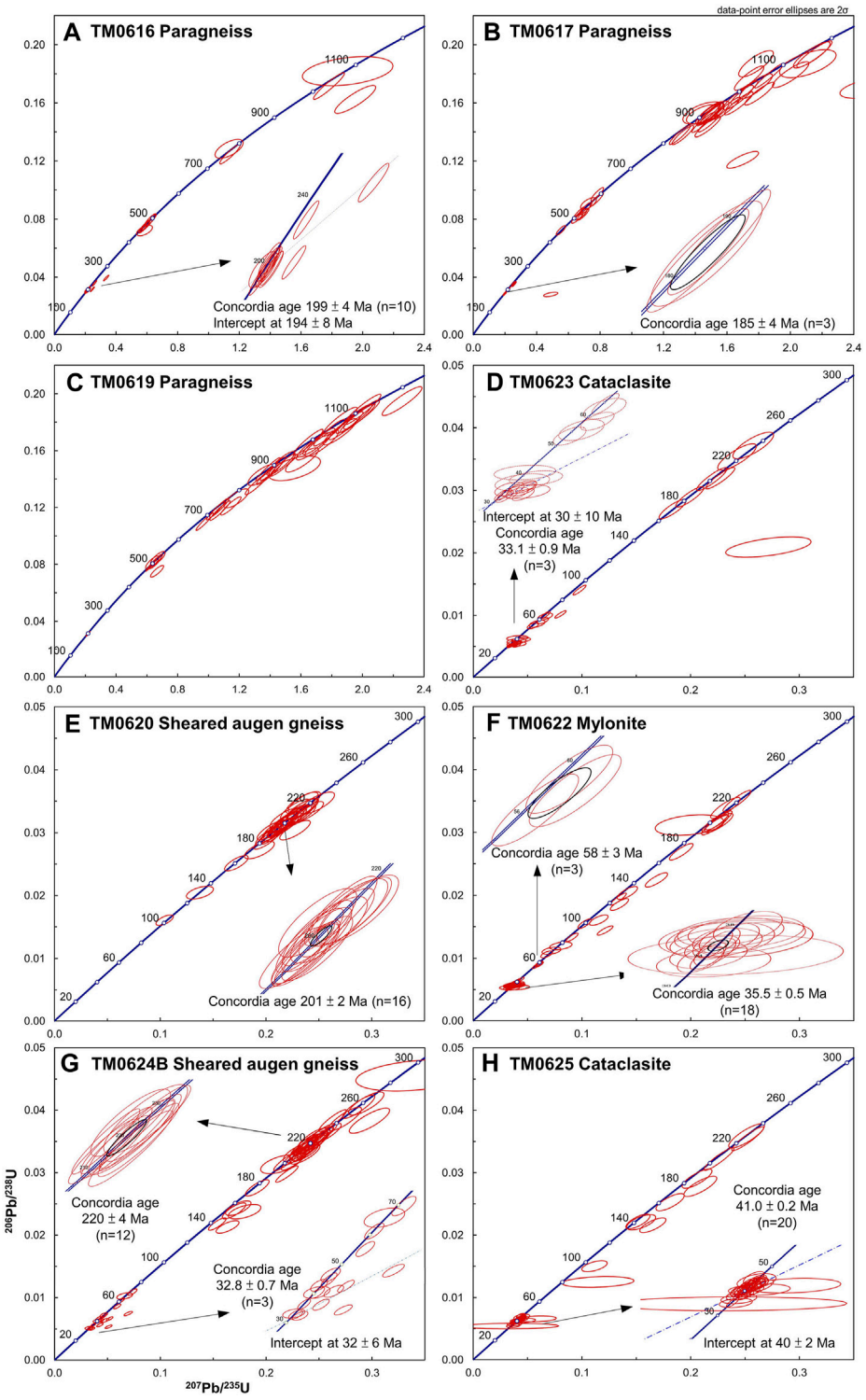


FIGURE 7
Zircon U-Pb concordia plots of the samples in this study. **(A–C)** paragneiss samples. **(D–H)** orthogneiss samples.

## 5.2 TM0617 paragneiss

In the TM0617 paragneiss, the plagioclase presents a fish-like grain shape coupled with bulging recrystallization, both markers of its ductile deformation (Figure 5B). Additionally, there are some brittle deformation textures present, such as grain size reduction, fractures, and domino structures. Plagioclase and K-feldspar porphyroclasts show alteration by sericite. Muscovite shows undulose extinction, bulging, and brittle deformation characterized by grain size reduction. Quartz shows dynamic recrystallization of BLG, SGR, and GBM.

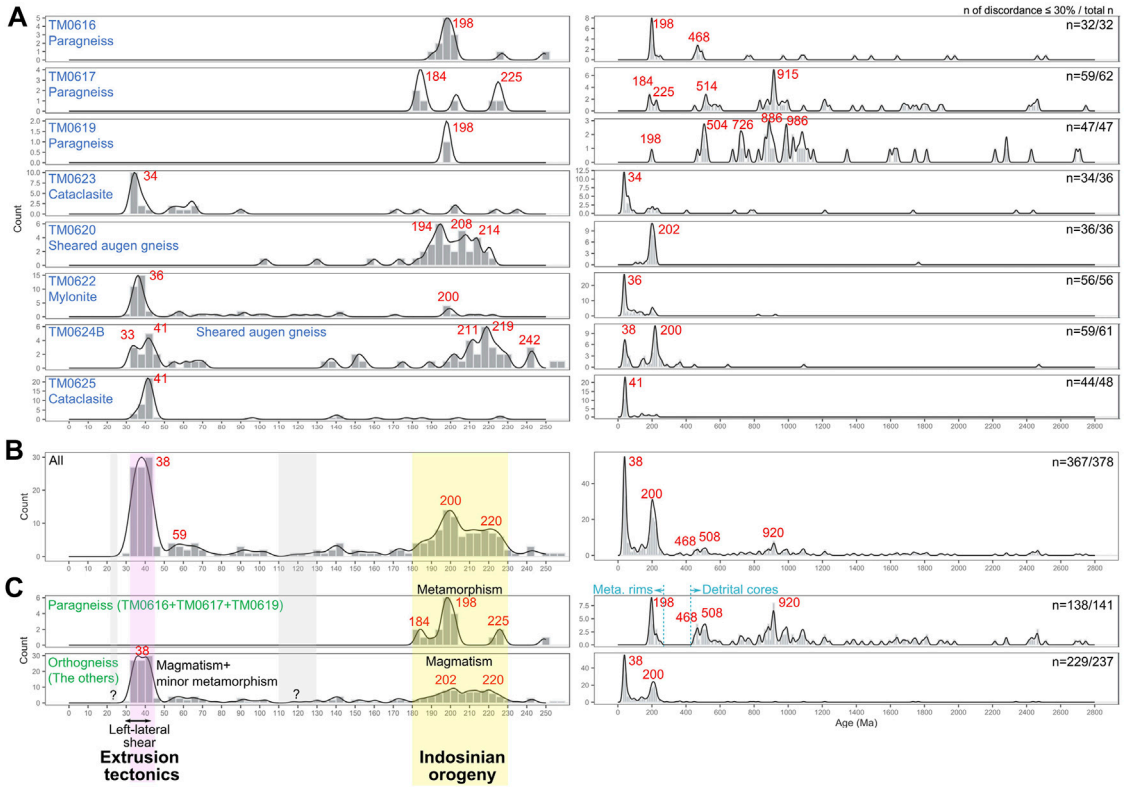


FIGURE 8
Kernel density estimate (KDE) plots of zircon U-Pb age spectra. The left panels are age spectra from 0-250 Ma, and the right panels are age spectra from 0-2,800 Ma **(A)** Age spectra for each sample **(B)** Age spectra of all analyses in this study **(C)** Age spectra for paragneiss and orthogneiss samples, respectively.

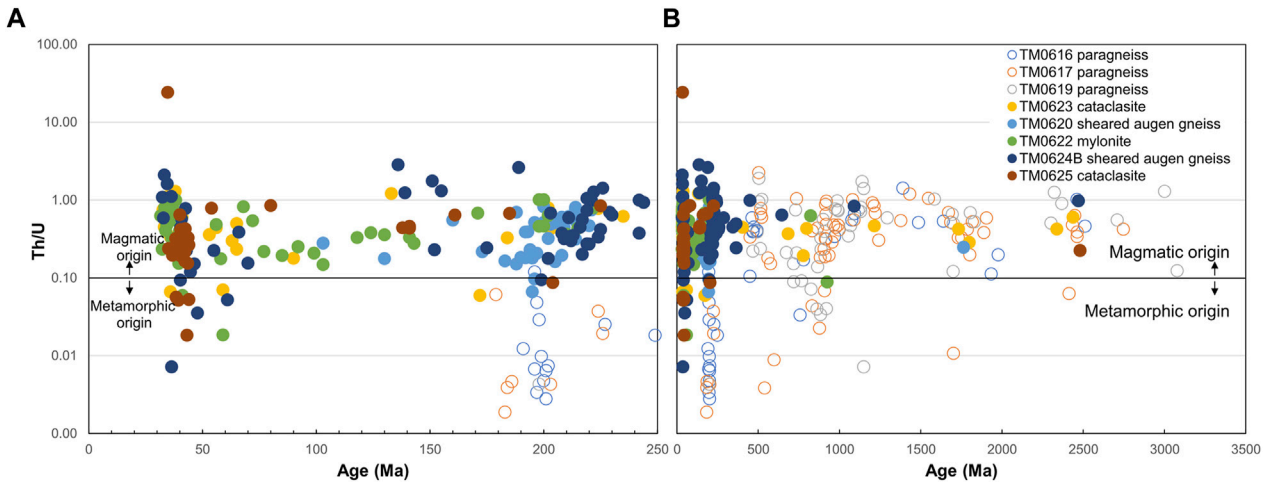


FIGURE 9
Zircon Th/U *versus* inferred ages for all analyses in this study **(A)** 0-250 Ma interval **(B)** 0-3,500 Ma interval. Most paragneiss zircon rims yield Th/U >0.01, indicating their metamorphic origin. The Eocene zircons predominantly have Th/U ratios >0.1, indicating their magmatic origins (Yakymchuk et al., 2018).

Zircons of TM0617 are sub-euhedral and short prismatic with a length of ~150 μm (Figure 6). SEM-CL images demonstrate that most of the zircons have bright and rounded cores with oscillatory zoning, overgrown by a thin layer of dull rims. A total of 62 analyses of 52 zircons yielded ages ranging from 2,747 to 179 Ma, clustered around 915, 514, 225, and 184 Ma (Figures 7B, 8A).

Zircon cores revealed ages of 2,747-450 Ma with an average Th/U ratio of 0.49 (Figure 9). Seven analyses on rims yielded ages of 226-179 Ma, and three of these yielded a concordia age of 185 ± 4 Ma (n=3, average Th/U=0.004).

## 5.3 TM0619 paragneiss

In the TM0619 paragneiss, quartz exhibits dynamic recrystallization characterized by BLG, SGR, and GBM (Figure 5C). Biotite contains kink bands. Deformation twinning, fish-like grain shape, and boudinage structure reveal ductile to brittle deformation of feldspar. Some myrmekite could be observed around the K-feldspar.

Zircons from sample TM0619 are predominantly rounded to short prismatic, measuring approximately 150 μm in length (Figure 6). SEM-CL images show their distinct oscillatory zoning patterns. A total of 47 analyses were conducted on this sample. Among them, only one analysis on a metamorphic rim was acquired due to the lack of a distinct core-rim structure in the other zircons. The rim age is 198 Ma with a Th/U ratio of 0.004. The remaining 46 analyses yielded U-Pb ages ranging from 3,078 to 467 Ma (Figures 7C, 8A), with the majority exhibiting Th/U ratios >0.1 (Figure 9).

One particular zircon displayed a 467 Ma core with a comparatively older 673 Ma rim. In fact, the core presented a higher age discordance of 10.9% compared to the rim's 2.7%. This could suggest that the core underwent greater Pb loss than the rim. Alternatively, the zircon could have grown during multiple events, which could lead to mixed signals from different generations or perhaps an improper selection of signal intervals during the analysis.

## 5.4 TM0623 cataclasite

The deformation of TM0623 cataclasite is primarily characterized by grain size reduction (Figure 5D). Feldspar porphyroclasts display deformation twinning, undulose extinction and fractures, indicating a progression of shear from plastic to brittle deformation.

Most zircons in this sample are euhedral to subhedral, long to short prismatic crystals with lengths of ~150 μm. They exhibit clear oscillatory zoning patterns (Figure 6). A total of 36 analyses were conducted on 33 zircon grains, resulting in U-Pb ages ranging from 2,438 to 32.6 Ma. Among these, six analyses yielded ages between 235 and 172 Ma, while another six analyses fell within the 65-53 Ma. Furthermore, 13 analyses yielded ages of 41-32.6 Ma, with a lower intercept age of 29.9 ± 9.6 Ma (Figure 7D). A concordia age of 33.1 ± 0.9 Ma could be calculated from three analyses. Most Eocene ages showed Th/U ratios >0.1 (Figure 9).

Analyses were conducted on both the core and rim of only three grains from this sample. Although some zircon grains showed clear, cloudy overgrowths, these were not sufficiently substantial to allow effective analyses.

## 5.5 TM0620 sheared augen gneiss

In TM0620 sheared augen gneiss, quartz displays dynamic recrystallization of BLG, SGR, and GBM (Figure 5E). Plagioclase porphyroclast exhibits deformation features such as plagioclase fish and deformation twinning, suggesting a deformation temperature of up to 600 °C. Fractures and grain size reduction of feldspars indicate subsequent brittle deformation. Biotite displays kink bands and grain size reduction. Sericite has formed inside and around the feldspar.

Zircons in this sample exhibit a subhedral, slightly rounded, long prismatic shape with lengths of 200–300 μm. (Figure 6). They share a similar oscillatory zoning pattern, characterized by a darker core, an intermediate cloudy layer, and the brightest thin crust on the SEM-CL images. A total of 36 analyses were performed, resulting in ages ranging from 1764 to 103 Ma. Most of the analyses clustered around 220-188 Ma (n = 30). Among them, 16 analyses yielded a concordia age of 201 ± 2 Ma with an average Th/U ratio of 0.37 (Figure 7E).

Out of 13 zircon grains for which both the core and rim were dated, nine of these grains had similar ages. One core distinctly presented an age of 1764 Ma, indicating its inherited nature, and its associated rim was dated to 192 Ma. Some grains exhibited rim ages older than their respective cores. This discrepancy could be due to the inadequate crosscutting of the zircon grains, resulting in a mixed signal from different generations, or to an improper selection of signal intervals during the analysis.

## 5.6 TM0622 mylonite

In the TM0622 mylonite, quartz shows dynamic recrystallization of BLG, SGR, and GBM (Figure 5F). Feldspar grains present as elongated and deformed, displaying bulging features. Some feldspar porphyroclasts exhibit boudinage structures. Sericite occurs within and around the feldspar.

Zircons in this mylonite sample are sub-euhedral and short prismatic crystals with a length of ~100 μm (Figure 6). SEM-CL images reveal that they have relatively simpler oscillatory zoning pattern. A total of 56 analyses were performed on 48 zircons, with U-Pb ages ranging mainly from 222 to 31.6 Ma, except for two significantly older ages of 924 and 823 Ma, respectively. Among these analyses, five yielded similar ages between 202 and 198 Ma, and three analyses resulted in ages of ~58 Ma (Figure 7F). A total of 29 analyses yielded ages ranging from 42.9 to 31.6 Ma, with Th/U ratios ranging from 0.15 to 1.00 (averaging 0.6, Figure 9) and a concordia age of 35.5 ± 0.5 Ma (n = 18).

Both core and rim analyses were performed on nine zircon grains for this sample. Four grains yielded similar Eocene-Oligocene ages from both the core and rim. One grain yielded the same age of 200 Ma for its core and rim. The remaining four grains displayed different ages in their core and rim. Their cores yielded Neoproterozoic or Late Triassic-Early Jurassic ages, while their rims were all Late Cretaceous.

## 5.7 TM0624B sheared augen gneiss

In the TM0624B sheared augen gneiss, quartz shows dynamic recrystallization of grain boundary area reduction (GBAR) to GBM (Figure 5G). Feldspar microstructures include bulging,

deformation twinning, myrmekitization, boudinage brittle deformation, and sericitic alteration.

Zircons in this sample are subhedral crystals with lengths of 100–200 μm (Figure 6). A total of 61 analyses were performed on 49 zircon grains, revealing ages ranging from 2,471 to 32 Ma. The age spectrum exhibited two prominent age clusters of 230–199 Ma and 48–32 Ma (Figure 7G). Of the analyses, 11 yielded a concordia age of 219.6 ± 3.8 Ma, with an average Th/U ratio of 0.57. Additionally, three analyses resulted in a concordia age of 32.8 ± 0.7 Ma with an average Th/U of 1.11. Five discordant analyses yielded a lower intercept age of 32 ± 6 Ma. These Eocene-Oligocene zircons exhibited high Th/U ratios, even exceeding those of the Triassic-Jurassic zircons.

Both core and rim analyses were performed on 12 zircon grains for this sample. Most grains yielded similar ages in both the core and rim, with the exception of two grains. One grain has an age of 1,089 Ma for its core and 43 Ma (Th/U=0.78) for its rim, while the other had ages of 221 and 152 Ma on its core and rim, respectively.

## 5.8 TM0625 cataclasite

TM0625 cataclasite has a high proportion of fine-grained material, which should result from grain size reduction, possibly due to its proximity to the MPSZ boundary fault (Figure 5H). Quartz displays dynamic recrystallization of GBAR to GBM. The elongated shape of feldspar porphyroclasts, along with undulose extinction and deformation twinning, indicate their plastic deformation. The presence of myrmekitization and sericitic alteration suggest that feldspar experienced deformation at temperatures up to 600°C (Passchier and Trouw, 2005). Biotite exists as fish and fine grains in the matrix, some pristine biotite can be found in the feldspars.

Zircon grains in this sample present as euhedral crystals with a length of ~100–200 μm. They display clear oscillatory zoning patterns on SEM-CL images (Figure 6). A total of 48 analyses were conducted, yielding ages ranging from 2,481 to 34.7 Ma. The majority of the analyses clustered around 45-35 Ma (n=35, Figure 7H). These Eocene zircons resulted in a concordia age of 41.0 ± 0.2 Ma (n=20) with an average Th/U ratio of 0.27.

# 6 Discussion

This study shows that the Lan Sang gneisses can be clearly divided into two main categories, paragneiss and orthogneiss, based on the geochronological evidence. This discovery reinforces the updated geological cross-section in Figure 4 of Österle et al. (2019). Therefore, we will discuss the formation and thermal history of paragneiss and orthogneiss separately.

## 6.1 Formation history of paragneisses

### 6.1.1 Paleozoic sedimentary protolith

Paragneiss samples TM0616, TM0617, and TM0619 were collected from the SW segment of the cross-section. Their zircon grains exhibit a distinct core-rim structure. Most cores have strong oscillatory zoning patterns (Figure 6) with Th/U ratios >0.1 (Figure 9), which may reflect their igneous origin (Belousova et al., 2002; Hoskin and Schaltegger, 2003). However, the rounded outlines (Figure 6) and wide U-Pb age span (3,078-450 Ma, Figures 8A,C) indicate that these cores may have experienced sedimentary processes prior to rim overgrowth. Therefore, these cores are likely to be detrital zircons. The youngest age of these detrital cores can be considered as the maximum depositional age for each corresponding sample (Dickinson and Gehrels, 2009), i.e., 462 Ma for TM0616, 450 Ma for TM0617, and 467 Ma for TM0619. This implies that the protoliths of these paragneisses could be Paleozoic sedimentary rocks.

Moreover, the age cluster of ~508 Ma suggests that the sediments of these paragneiss protoliths primarily came from the Sibumasu terrane rather than the Indochina terrane (Lin et al., 2013; Kawakami et al., 2014; Dew et al., 2018). The age spectrum of detrital zircon cores in this study is also similar to that of Paleozoic sedimentary rocks from the Sibumasu terrane (Dew et al., 2021; Hara et al., 2021). Considering that the MPSZ is flanked by Cambrian quartzite and Permian limestone (Figure 3), it seems reasonable to infer that the protoliths of these paragneisses should be Paleozoic sedimentary rocks around the Sibumasu terrane.

### 6.1.2 Paragneiss formation in the Triassic-Jurassic metamorphism

On the other hand, zircon rims exhibit dull and cloudy zonation without an oscillatory zoning pattern on the SEM-CL images, very low Th/U ratios (average of 0.02, Figure 9), and a lower intercept age (194 ± 8 Ma of TM0617). These suggest that these zircon rims should be metamorphic overgrowth (Hoskin and Black, 2000; Rubatto, 2002; Blackburn et al., 2011; Rubatto, 2017; Yakymchuk et al., 2018). These zircon rims reveal ages of around 249, 227-183, and 179 Ma (Figure 8C), with the exception of one analysis that yields 449 Ma (Th/U=0.1) in TM0616. This exception may be due to another generation of zircon overgrowth or the mixed core and rim signal. Analyses of 249 and 179 Ma lack repeatable data, and their age discordances (18% and 125%, respectively) are also much greater than others (mostly <4%). These two analyses probably result from the mixed signals of distinct zircon generations and severe Pb loss, respectively. Thus, they should not be considered a representation of the zircon overgrowth.

Similar zircon U-Pb ages of metamorphic zircon rims from two Lan Sang gneiss samples have been reported as 191 ± 10 and 206 ± 4 Ma (Kanjanapayont et al., 2011). These dates are consistent with our ages of 227-183 Ma for the metamorphic zircon rims. The lower intercept ages of approximately 200 Ma revealed by Ahrendt et al. (1993) and by TM0617 paragneiss in this study further substantiate the presence of this metamorphic event.

To summarize, the observed overgrowth rim on the zircons is indicative of metamorphism that occurred between 227 and 183 Ma, consistent with the Indosinian orogeny. This metamorphism is believed to have played a role in the transformation of sedimentary protoliths into paragneiss.

## 6.2 Thermal history revealed by orthogneiss samples

Orthogneiss samples include TM0623 cataclasite, TM0620 sheared augen gneiss, TM0622 mylonite, TM0624B sheared augen gneiss,

and TM0625 cataclasite. Most of their zircons exhibit euhedral to subhedral shapes with oscillatory zoning and high Th/U ratio (most >0.2, Figure 9), suggesting their igneous origins (Belousova et al., 2002; Hoskin and Schaltegger, 2003). These zircons yield primarily either Triassic-Jurassic or Eocene-Oligocene ages, with a few older ages (Figure 8C). The presence of older ages could be attributed to inherited zircons or mixed ages partially involving inherited zircons. Only the TM0624B sheared augen gneiss sample presents zircons from both age groups.

### 6.2.1 Triassic-Jurassic magmatism

The age distribution of the TM0624B sheared augen gneiss is similar to that of the TH0101 II augen gneiss sample in Österle et al. (2019), with more Triassic-Jurassic zircons than Eocene-Oligocene zircons. However, the high Th/U ratios and the similarities between the core and rim ages suggest that the Eocene-Oligocene zircons may not have originated from metamorphism. In contrast, these zircons yield a lower intercept age of 32 ± 6 Ma on the concordia plot (Figure 7G), which is often regarded as a metamorphic age, complicating the interpretation. Indeed, there are instances where metamorphic zircons can exhibit Th/U values greater than 0.1. This can occur in recrystallized zircons, zircons grown during high-T metamorphism, or zircons derived from syn-metamorphic, high-T anatectic melts (Schaltegger et al., 1999; Harley et al., 2007; Yakymchuk et al., 2018). Considering the scattered distribution of Eocene-Oligocene dates and a lower intercept on the concordia plot (Figure 7G), the protolith was likely emplaced during the Triassic-Jurassic period (230–199 Ma) and experienced high-T metamorphism, in addition to ductile deformation, by 32 Ma.

Among all samples, the TM0620 sheared augen gneiss is characterized by the largest zircon grain size, and its zircons predominantly exhibit Triassic-Jurassic ages. The protolith of TM0620 should be emplaced between 220 and 188 Ma. The precise timing of its gneiss formation remains unclear due to the absence of metamorphic zircons or a lower intercept age.

Rb-Sr whole rock isochron ages of 219-213 Ma have been reported for Tak granite, east of the MPSZ (Teggin, 1975). Zircon U-Pb dating on augen gneiss of the Lan Sang gneisses revealed that the protolith may have intruded at around 208 Ma (Österle et al., 2019). These ages fit well with magmatic ages of 221-210 Ma for the Chiang Mai-Lincang granitoid and gneiss belt (Dunning et al., 1995; Macdonald et al., 2010; Gardiner et al., 2016). Therefore, it is undoubtedly confirmed that some Lan Sang gneisses had protolith emplacement during the Triassic-Jurassic.

### 6.2.2 Eocene-Oligocene magmatism

On the other hand, zircons within the TM0623 cataclasite, TM0622 mylonite, and TM0625 cataclasite exhibit predominantly concordant Eocene-Oligocene ages (45-32 Ma) with high Th/U values (Figures 7D,F,H). These zircons also show euhedral to subhedral shapes and clear oscillatory zoning patterns in the SEM-CL images (Figure 6). Thus, these features indicate that these zircons should be of igneous origin (Belousova et al., 2002; Hoskin and Schaltegger, 2003).

Palin et al. (2013) proposed that the event that occurred between 45 and 37 Ma in the MPSZ was a metamorphism, supported by the presence of metamorphic features observed in the dated monazite. Österle et al. (2019) proposed that this metamorphism, initiated at ~45 Ma, culminated in the partial melting of the basement and granodioritic intrusion at ~35 Ma. However, we introduce a new perspective based on our new zircon U-Pb results. The thermal event that occurred at 45 Ma and continued until 32 Ma, was not merely a metamorphic event. Rather, it is indicative of a magmatic event, supported by the spatial distribution of samples containing igneous zircons from 45-32 Ma within the MPSZ (Figure 3).

### 6.2.3 Eocene-Oligocene metamorphism

Further evidence from the lower intercepts on the concordia of TM0623 and TM0624B (Figures 7D,G) suggests that the associated metamorphism likely terminated at around 32–30 Ma. This extended period of metamorphism may have resulted from cooling due to the cessation of magmatic activity. This corroborates the cooling phase as evidenced by biotite K/Ar ages of 31.9–29.9 Ma, biotite $^{40}Ar/^{39}Ar$ ages of 33-30.6 Ma, K-feldspar $^{40}Ar/^{39}Ar$ ages of 35.4–30.5 Ma, zircon fission track ages of 35.9-28 Ma (Ahrendt et al., 1993; Lacassin et al., 1997; Morley et al., 2007; Lin et al., 2021).

Furthermore, in TM0623, TM0622, and TM0625, K-felspar porphyroclasts have been replaced by muscovite, biotite, or albite, indicating the occurrence of a Na-K exchange reaction. This reaction is known to occur at temperatures of 490°C–750 °C and pressures of 2–13 kbar in peraluminous granitoids (Green and Usdansky, 1986). This observation supports the presence of metamorphism following the Eocene-Oligocene magmatism.

## 6.3 Possibilities of other magmatic events

Zircon age spectra of paragneisses (TM0616, TM0617, and TM0619) reveal minor age clusters at ~920 Ma and ~508-468 Ma (Figure 8C). These ages are derived from detrital zircon cores, indicating they may provide insight into sedimentary provenance. Prior to the earliest zircon U-Pb dating studies (i.e., Ahrendt et al., 1993; MacDonald et al., 1993; Dunning et al., 1995), it was believed that Thailand had Precambrian basement rocks due to its overlying Cambrian sedimentary rocks (Hansen and Wemmer, 2011). However, subsequent zircon U-Pb dating studies have revealed that most of the crystalline basement rocks in Thailand are of Indosinian age (Dunning et al., 1995; Kawakami et al., 2014; Gardiner et al., 2016; Dew et al., 2018). Only a few outcrops in peninsular Thailand have yielded the oldest magmatic ages of ca. 500 Ma, revealing that the Sibumasu terrane was in a magmatic arc-related regime on the Gondwana India-Australia margin (Lin et al., 2013; Kawakami et al., 2014; Dew et al., 2018). The exact location of the Precambrian basement rock remains unknown, with only clues from inherited and detrital zircon ages (Ahrendt et al., 1993; Watkinson et al., 2011; Cai et al., 2017; Dew et al., 2018; Österle et al., 2019; Dew et al., 2021; Hara et al., 2021). The majority of detrital zircon age spectra obtained from sedimentary and meta-sedimentary rocks in the Sibumasu terrane also exhibit a prominent peak either at 500 Ma or within 1,000-900 Ma (Cai et al., 2017; Dew et al., 2021; Hara et al., 2021). This finding strongly indicates the presence of Neoproterozoic basement rocks in the Sibumasu terrane.

Although the monazite U-Th-Pb geochronology study suggested that the magmatic protolith of the Lan Sang orthogneiss may have been emplaced between 123 and 114 Ma

(Palin et al., 2013), neither the previous zircon U-Pb dating studies (Ahrendt et al., 1993; Kanjanapayont et al., 2011; Österle et al., 2019) nor this study revealed a notable zircon U-Pb age cluster from this period. The two analyses of 123-114 Ma from monazite cores by Palin et al. (2013) probably resulted from a minor metamorphic event or localized intrusion.

This study did not find a date of 22 Ma, an age previously identified from an undeformed subvolcanic dike by Österle et al. (2019). This is likely due to the fact that our samples primarily comprised deformed rocks rather than undeformed ones.

## 6.4 Relationship between Eocene-Oligocene magmatism and shear activity

The ages obtained from TM0623 cataclasite (41-32.6 Ma), TM0622 mylonite (42.9–31.6 Ma), and TM0625 cataclasite (45-35 Ma), which are mainly from igneous zircons, closely coincide with the proposed shearing duration of 42-30 Ma for the MPSZ (Lin et al., 2021). This suggests that these samples can be syn-shearing intrusions, supporting the findings in Österle et al. (2019).

Magmatism between 45 and 32 Ma appears to slightly precede the left-lateral shearing along the MPSZ between 42 and 30 Ma (Lin et al., 2021). This discrepancy could be attributed to the differences in closure temperatures tied to the respective geochronological methods and to the uncertainty in determining the onset of shearing. Based on calculations and field-based estimates, the closure temperatures for Pb diffusion in zircon of typical size exceed 900 °C (Mezger and Krogstad, 1997; Cherniak and Watson, 2001). Thus, the U-Pb age of igneous zircon usually represents the crystallization age and provides the exact timing of a magmatic event. The closure temperature for Ar diffusion in muscovite ranges from 425°C to 350 °C (Hodges, 1991; Harrison et al., 2009), varying based on grain size, cooling rate, and pressure. When muscovite crystallizes or recrystallizes at a temperature below its closure temperature due to deformation (West and Lux, 1993; Reddy and Potts, 1999), or when it deforms during cooling from a high temperature to beneath its closure temperature (Lin et al., 2021), it can record a deformation age. Consequently, determining the timing of deformation is always challenging, and identifying the precise onset of deformation proves to be even more difficult.

Microstructures in thin sections indicate that the left-lateral shear occurred at high temperatures, likely in excess of 600°C, and persisted into the low-temperature brittle regime characterized by fracturing and cataclasis. This observation is consistent with the estimated deformation temperature range of >600°C to 250°C, derived from the deformation microstructures of various minerals and the recrystallized grain size of quartz in the sheared leucogranite (Lin et al., 2021). Therefore, the onset of the MPSZ is likely to have occurred earlier than 42 Ma, as indicated by the $^{40}Ar/^{39}Ar$ muscovite age with a calculated closure temperature of ~435°C (Lin et al., 2021).

The emplacement of the intrusion has been observed in close spatial and temporal association with shear or fault activity (Pitcher and Bussell, 1977; Neves et al., 1996; Brown and Solar, 1998; Rosenberg, 2004). The development of S-C fabrics within granitoids, which were emplaced in the shear zone, indicates that incompletely solidified plutons can induce strain localization and favor shear zone nucleation due to rheological heterogeneities (Tommasi et al., 1994; Neves et al., 1996; Brown and Solar, 1998). Therefore, the syn-shearing intrusion of TM0623 cataclasite, TM0622 mylonite, and TM0625 cataclasite may have experienced greater strain compared to the country rock. As a result, these samples contain a higher proportion of fine-grained material compared to the other two sheared augen gneiss samples, which were emplaced during the Triassic-Jurassic.

Alternatively, shear heating has been proposed to cause partial melting and metamorphism (Fleitout and Froidevaux, 1980; Leloup and Kienast, 1993). Recent studies show that shear heating can increase temperature by 50°C–200°C (Duretz et al., 2014; Mako and Caddick, 2018). Although the temperature increase caused by shear heating alone may not be sufficient to induce partial melting and metamorphism, it may still contribute to these processes (Strong and Hanmer, 1981). Therefore, the contemporaneous intrusion and shear activity of the MPSZ may not be merely a coincidence.

Our deformed samples show a lack of ages around 22 Ma (Figure 8B), an age previously identified from an undeformed subvolcanic dike by Österle et al. (2019). This suggests that the left-lateral shearing of the MPSZ likely ceased before 22 Ma. Considering the shearing duration of 42-30 Ma as constrained by thermochronology (Lin et al., 2021), it is probable that the cessation of left-lateral shearing within the MPSZ occurred between 30 and 22 Ma.

## 6.5 Distribution of the Eocene-Oligocene magmatism along the Sibumasu terrane

Apart from the MPSZ, Eocene-Oligocene magmatic events have also been discovered in other areas of the Sibumasu terrane (Figure 10). In the northernmost part of the Sibumasu terrane, the emplacement of the Cangyuan granitoid took place at 45-40 Ma (Deng et al., 2014, and references therein). In northern Thailand, the granitic mylonite of the Doi Suthep core complex has yielded zircon and monazite U-Pb ages of 40 Ma (Macdonald et al., 2010), while a calc-silicate gneiss near the Doi Inthanon metamorphic core complex has shown a zircon age of 27 Ma (Dunning et al., 1995). Moreover, samples of biotite augen gneiss between the Doi Suthep and the Doi Inthanon complexes have revealed zircon and monazite U-Pb ages of 32-26 and 34-24 Ma, respectively. These ages indicate metamorphism and anatexis associated with crustal thickening, which has been used to infer a model for the onset of extension and subsequent development of the Chiang Mai Basin (Gardiner et al., 2016).

Zircon U-Pb dating of orthogneiss and mylonite samples from the TPSZ yields ages of 59-48 Ma (Nantasin et al., 2012). Zircons from a foliated biotite-hornblende granite of the RSZ have been dated, revealing ages of 50–44 Ma (Watkinson et al., 2011). Orthogneisses, mylonitic granite, and pegmatites of the KMSZ have zircon U-Pb ages of 55-46 Ma, which may be linked to an early dextral ductile deformation phase (Kanjanapayont et al., 2012). In southeastern Thailand, magmatic zircon U-Pb ages of 55-43.3 Ma have been obtained from monzogranite and granite samples (Veeravinantanakul et al., 2021; Uchida et al., 2022). Veeravinantanakul et al. (2021) interpreted 43 Ma as the timing of intrusion during the sinistral movement of the KSZ.

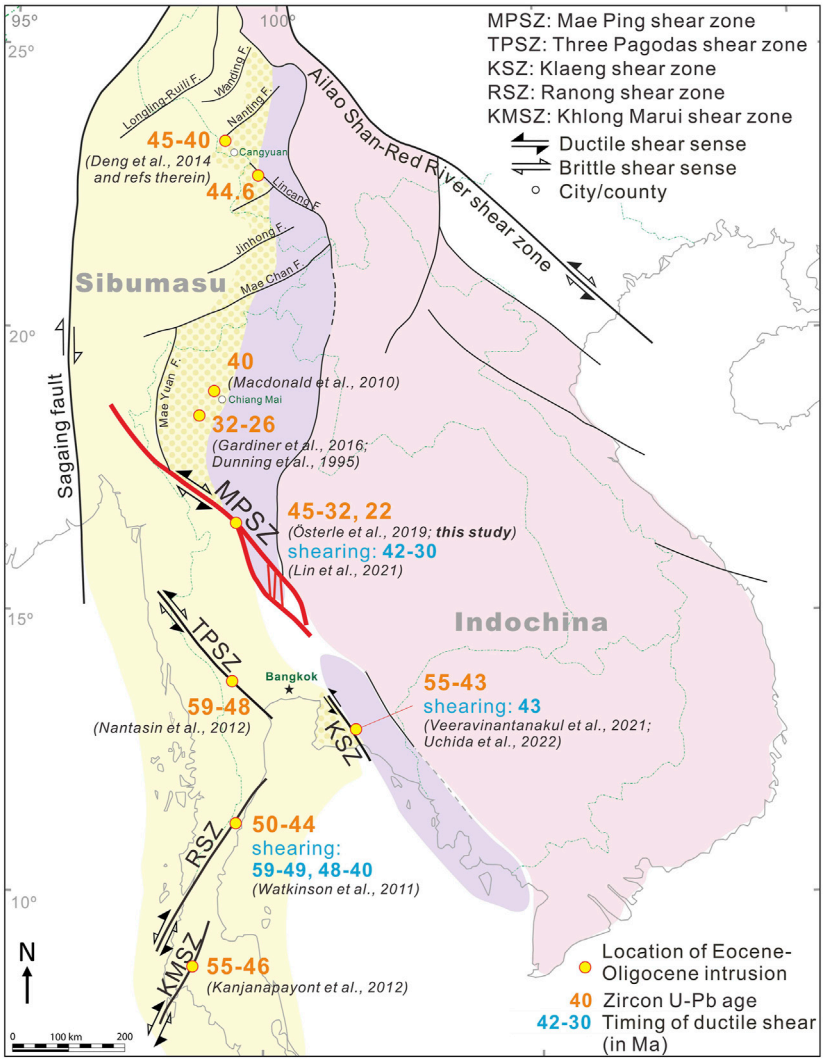


FIGURE 10
Distribution of Eocene-Oligocene intrusions along the Sibumasu terrane. The Eocene-Oligocene intrusions were mainly found within the shear zones or fault zones. Zircon U-Pb ages and the inferred shear durations are from this study and the literature (Dunning et al., 1995; Macdonald et al., 2010; Watkinson et al., 2011; Kanjanapayont et al., 2012; Nantasin et al., 2012; Deng et al., 2014; Gardiner et al., 2016; Österle et al., 2019; Lin et al., 2021; Veeravinantanakul et al., 2021; Uchida et al., 2022).

The prevalence of Eocene-Oligocene magmatism along the Sibumasu terrane may have significantly impacted the regional cooling history. Morley et al. (2007) observed a predominantly N-S trend in the regional cooling patterns of northwestern Thailand as shown by biotite, ZFT, and AFT ages. They proposed that the exposure of the Lan Sang gneisses is more intimately linked with regional exhumation patterns than being solely attributable to strike-slip-induced uplift and erosion (Morley et al., 2007). Palin et al. (2013) also suggested that the strike-slip motion of the MPSZ was not directly responsible for either the metamorphism or regional cooling. The distribution of Eocene-Oligocene magmatism in the Sibumasu terranes (Figure 10) is consistent with the observed N-S trend in the regional cooling pattern (Figure 5 in Morley et al., 2007) and the timing of metamorphism. These findings indicate that Eocene-Oligocene magmatism likely contributed to the contemporaneous metamorphic processes and regional cooling patterns.

The Eocene-Oligocene magmatism in the Sibumasu terrane corresponds well with the period of reduced magmatism (45-30 Ma) in the Neo-Tethyan arc system, which includes Gangdese, West Burma, and Sumatra (Zhang et al., 2019). The reduced magmatism in the Neo-Tethyan arc system and the magmatism in the Sibumasu during the Eocene-Oligocene may not be merely a coincidence. They could be correlated with the tectonic scenario involving the shallowing slab of the Neo Tethys, which would induce magmatism migration from West Burma to the Sibumasu terrane (Zhang et al., 2019).

In addition to the quiescence of arc magmatism and inward migration of magmatism on the overriding plate, shallowing slab or flat subduction may also have resulted in strong compression, leading to crustal thickening, metamorphism, and strike-slip motion on the overriding plate (Kay and Coira, 2009; Lee and King, 2011; Zhang et al., 2019). The inferred shear timing of the MPSZ, RSZ, and KSZ is similar to their corresponding magmatic ages (Figure 10). This can be attributed to the fact that magmatism can soften the lithosphere,

promote strain localization, and favor shear zone nucleation (Neves et al., 1996; Brown and Solar, 1998). One experimental study proposed that the crustal-scale localization of deformation effectively coincides with the onset of melting (Rosenberg and Handy, 2005). It is important to note that magmatism, metamorphism, and deformation may be interconnected or promote each other in the context of convergent tectonic settings, allowing them to occur simultaneously (Hutton and Reavy, 1992; Rosenberg, 2004; Rosenberg and Handy, 2005).

## 7 Conclusion

This study presents new zircon U-Pb age data, revealing that the magmatic history of the MPSZ was dominated by Triassic-Jurassic and Eocene-Oligocene thermal events. Paragneiss samples with Paleozoic sedimentary protoliths, mainly sourced from the Sibumasu terrane, underwent high-grade metamorphism during the Triassic-Jurassic Indosinian orogeny. The protoliths of the orthogneiss samples were emplaced either during the Triassic-Jurassic or the Eocene-Oligocene. The Eocene-Oligocene thermal event commenced at least at 45 Ma and ceased at 32 Ma. This event, previously recognized as a metamorphism, is now evidenced to be magmatism. Given that all samples were left-laterally sheared, the left-lateral motion of the MPSZ may have ended after the youngest zircon age, i.e., 32 Ma, corroborating previous findings.

Moreover, the Eocene-Oligocene magmatism in the MPSZ was probably not confined to a localized occurrence. Concurrent magmatic activities occurred in various regions within the Sibumasu terrane, i.e., Cangyuan, the Doi Inthanon and Doi Suthep areas, the TPSZ, KSZ, RSZ, and KMSZ. The close temporal and spatial correlation between magmatism and shear zones indicates that the occurrence of magmatism may be associated with shear activity. The Cenozoic regional cooling patterns of northern Thailand now appear to have been influenced by this magmatism. Furthermore, the distribution of Eocene-Oligocene magmatism along the Sibumasu terrane supports the possibility of an inward migration of magmatism within the overriding plate, moving from West Burma towards the Sibumasu terrane, probably due to the slab shallowing of the Neo-Tethyan. This slab shallowing may have induced strain within the Sibumasu. The occurrence of Eocene-Oligocene magmatism may have further weakened the lithosphere, thereby promoting strain concentration along the shear zones. Although metamorphism and regional cooling may not exhibit a direct relationship with shear deformation, these processes may be tectonically interconnected through the presence of magmatism.

## Data availability statement

The original contributions presented in the study are included in the article/Supplementary Material, further inquiries can be directed to the corresponding authors.

## Author contributions

Y-LL was responsible for data reduction and manuscript writing with support from T-YL. T-YL and PC conducted the field trip and sample collection. Y-LL, H-YL, and YI conducted the experiments. All authors contributed to the article and approved the submitted version.

## Funding

This research was supported by grants to Y-LL (MOST 110-2811-M-003-536) and T-YL (MOST 108-2116-M-003-007-MY3) from the Ministry of Science and Technology (now NCST), Taiwan.

## Acknowledgments

The authors are grateful to Prof. Meng-Wan Yeh for field work, sample collection, and laboratory equipment. Special thanks to Han-Yi Chiu, Chien-Hui Hung, Jia-Hui Chen, and Yi-Ju Hsin for guidance in zircon target fabrication, LA-ICP-MS operation, and data reduction. The careful review and constructive comments provided by Prof. K. R. Hari and Dr. Thuy Thanh Pham are gratefully acknowledged. The authors thank J. Gregory Shellnutt for editorial assistance.

## Conflict of interest

The authors declare that the research was conducted in the absence of any commercial or financial relationship that could be construed as a potential conflict of interest.

The handling editor JGS declared a past co-authorship with the authors TYL, HYL & YL.

## Publisher's note



## Supplementary material

The Supplementary Material for this article can be found online at: https://www.frontiersin.org/articles/10.3389/feart.2023.1213958/full#supplementary-material

## References

Ahrendt, H., Chonglakmani, C., Hansen, B. T., and Helmcke, D. (1993). Geochronological cross section through northern Thailand. *J. Southeast Asian Earth Sci.* 8, 207–217. doi:10.1016/0743-9547(93)90022-h

Andersen, T., Kristoffersen, M., and Elburg, M. A. (2018). Visualizing, interpreting and comparing detrital zircon age and Hf isotope data in basin analysis – A graphical approach. *Basin Res.* 30 (1), 132–147. doi:10.1111/bre.12245

Arboit, F., Collins, A. S., Morley, C. K., King, R., and Amrouch, K. (2016). Detrital zircon analysis of the southwest Indochina terrane, central Thailand: unravelling the indosinian orogeny. *GSA Bull.* 128 (5-6), 1024–1043. doi:10.1130/B31411.1

Belousova, E., Griffin, W., O'Reilly, S. Y., and Fisher, N. (2002). Igneous zircon: trace element composition as an indicator of source rock type. *Contrib. Mineral. Petrol.* 143 (5), 602–622. doi:10.1007/s00410-002-0364-7

Blackburn, T., Bowring, S. A., Schoene, B., Mahan, K., and Dudas, F. (2011). U-Pb thermochronology: creating a temporal record of lithosphere thermal evolution. *Contrib. Mineral. Petrol.* 162 (3), 479–500. doi:10.1007/s00410-011-0607-6

Brown, M., and Solar, G. S. (1998). Shear-zone systems and melts: feedback relations and self-organization in orogenic belts. *J. Struct. Geol.* 20 (2-3), 211–227. doi:10.1016/S0191-8141(97)00068-0

Cai, F., Ding, L., Yao, W., Laskowski, A. K., Xu, Q., Zhang, J. e., et al. (2017). Provenance and tectonic evolution of lower paleozoic–upper mesozoic strata from Sibumasu terrane, Myanmar. *Gondwana Res.* 41, 325–336. doi:10.1016/j.gr.2015.03.005

Cherniak, D. J., and Watson, E. B. (2001). Pb diffusion in zircon. *Chem. Geol.* 172 (1), 5–24. doi:10.1016/S0009-2541(00)00233-3

Chiu, H. Y., Chung, S. L., Wu, F. Y., Liu, D., Liang, Y. H., Lin, I. J., et al. (2009). Zircon U-Pb and Hf isotopic constraints from eastern Transhimalayan batholiths on the precollisional magmatic and tectonic evolution in southern Tibet. *Tectonophysics* 477 (1–2), 3–19. doi:10.1016/j.tecto.2009.02.034

Chung, S. L., Searle, M. P., and Yeh, M. W. (2008). The age of the potassic alkaline igneous rocks along the Ailao Shan–Red River shear zone: implications for the onset age of left-lateral shearing: A discussion. *J. Geol.* 116 (2), 201–204. doi:10.1086/527458

Deng, J., Wang, Q., Li, G., and Santosh, M. (2014). Cenozoic tectono-magmatic and metallogenic processes in the Sanjiang region, southwestern China. *Earth-Science Rev.* 138, 268–299. doi:10.1016/j.earscirev.2014.05.015

Dew, R. E. C., Collins, A. S., Glorie, S., Morley, C. K., Blades, M. L., Nachtergaele, S., et al. (2018). Probing into Thailand's basement: new insights from U–Pb geochronology, Sr, Sm–Nd, Pb and Lu–Hf isotopic systems from granitoids. *Lithos* 320-321, 332–354. doi:10.1016/j.lithos.2018.09.019

Dew, R. E. C., Collins, A. S., Morley, C. K., King, R. C., Evans, N. J., and Glorie, S. (2021). Coupled detrital zircon U–Pb and Hf analysis of the Sibumasu terrane: from Gondwana to northwest Thailand. *J. Asian Earth Sci.* 211, 104709. doi:10.1016/j.jseaes.2021.104709

Dickinson, W. R., and Gehrels, G. E. (2009). Use of U–Pb ages of detrital zircons to infer maximum depositional ages of strata: A test against a Colorado plateau mesozoic database. *Earth Planet. Sci. Lett.* 288 (1), 115–125. doi:10.1016/j.epsl.2009.09.013

DMR (1999). *Geological map of Thailand 1:2,500,000*. Bangkok, Thailand: Geological Survey Division, Department of Mineral Resources.

Dunning, G. R., Macdonald, A. S., and Barr, S. M. (1995). Zircon and monazite U-Pb dating of the Doi inthanon core complex, northern Thailand: implications for extension within the indosinian orogen. *Tectonophysics* 251 (1-4), 197–213. doi:10.1016/0040-1951(95)00037-2

Duretz, T., Schmalholz, S., Podladchikov, Y., and Yuen, D. (2014). Physics-controlled thickness of shear zones caused by viscous heating: implications for crustal shear localization. *Geophys. Res. Lett.* 41, 4904–4911. doi:10.1002/2014GL060438

Fleitout, L., and Froidevaux, C. (1980). Thermal and mechanical evolution of shear zones. *J. Struct. Geol.* 2 (1), 159–164. doi:10.1016/0191-8141(80)90046-2

Gardiner, N. J., Roberts, N. M. W., Morley, C. K., Searle, M. P., and Whitehouse, M. J. (2016). Did Oligocene crustal thickening precede basin development in northern Thailand? A geochronological reassessment of Doi inthanon and Doi Suthep. *Lithos* 240-243, 69–83. doi:10.1016/j.lithos.2015.10.015

Green, N. L., and Usdansky, S. I. (1986). Toward a practical plagioclase-muscovite thermometer. *Am. Mineral.* 71 (9-10), 1109–1117.

Hansen, B. T., and Wemmer, K. (2011). "Age and evolution of the basement rocks in Thailand," in *The Geology of Thailand*. Editors M. F. Ridd, A. J. Barber, and M. J. Crow (London: Geological Society), 19–32.

Hara, H., Tokiwa, T., Kurihara, T., Charoentitirat, T., and Sardsud, A. (2021). Revisiting the tectonic evolution of the Triassic Palaeo-Tethys convergence zone in northern Thailand inferred from detrital zircon U–Pb ages. *Geol. Mag.* 158 (5), 905–929. doi:10.1017/S0016756820001028

Harley, S. L., Kelly, N. M., and Moller, A. (2007). Zircon behaviour and the thermal histories of mountain chains. *Elements* 3 (1), 25–30. doi:10.2113/gselements.3.1.25

Harrison, T. M., Célérier, J., Aikman, A. B., Hermann, J., and Heizler, M. T. (2009). Diffusion of $^{40}$Ar in muscovite. *Geochimica Cosmochimica Acta* 73 (4), 1039–1051. doi:10.1016/j.gca.2008.09.038

Hodges, K. V. (1991). Pressure-temperature-time paths. *Annu. Rev. Earth Planet. Sci.* 19 (1), 207–236. doi:10.1146/annurev.ea.19.050191.001231

Hoskin, P. W. O., and Black, L. P. (2000). Metamorphic zircon formation by solid-state recrystallization of protolith igneous zircon. *J. Metamorph. Geol.* 18 (4), 423–439. doi:10.1046/j.1525-1314.2000.00266.x

Hoskin, P. W. O., and Schaltegger, U. (2003). The composition of zircon and igneous and metamorphic petrogenesis. *Rev. Mineral. Geochem.* 53 (1), 27–62. doi:10.2113/0530027

Hutton, D. H. W., and Reavy, R. J. (1992). Strike-slip tectonics and granite petrogenesis. *Tectonics* 11 (5), 960–967. doi:10.1029/92TC00336

Jarvis, A., Reuter, H. I., Nelson, A., and Guevara, E. (2008). *Hole-filled SRTM for the globe version 4.* available from the CGIAR-CSI SRTM 90m Database (http://srtm.csi.cgiar.org).

Kanjanapayont, P., Klötzli, U., Charusiri, P., and Klötzli, E. (2011). "LA-MC-ICP-MS UPb zircon geochronology of the lan Sang and nong yai gneisses, Thailand," in International Conference on Geology, Geotechnology and Mineral Resources of Indochina (GEOINDO 2011).

Kanjanapayont, P., Klötzli, U., Thöni, M., Grasemann, B., and Edwards, M. A. (2012). Rb–Sr, Sm–Nd, and U–Pb geochronology of the rocks within the Khlong Marui shear zone, southern Thailand. *J. Asian Earth Sci.* 56 (0), 263–275. doi:10.1016/j.jseaes.2012.05.029

Kanjanapayont, P., Kieduppatum, P., Klötzli, U., Klötzli, E., and Charusiri, P. (2013). Deformation history and U–Pb zircon geochronology of the high grade metamorphic rocks within the Klaeng fault zone, eastern Thailand. *J. Asian Earth Sci.* 77, 224–233. doi:10.1016/j.jseaes.2013.08.027

Kawaguchi, K., Minh, P., Hieu, P. T., Cuong, T. C., and Das, K. (2021). Evolution of supracrustal rocks of the Indochina block: evidence from new detrital zircon U–Pb ages of the kontum massif, central vietnam. *J. Mineral. Petrol. Sci.* 116 (2), 69–82. doi:10.2465/jmps.200916

Kawakami, T., Nakano, N., Higashino, F., Hokada, T., Osanai, Y., Yuhara, M., et al. (2014). U-Pb zircon and CHIME monazite dating of granitoids and high-grade metamorphic rocks from the Eastern and Peninsular Thailand- A new report of Early Paleozoic granite. *Lithos* 200-201, 64–79. doi:10.1016/j.lithos.2014.04.012

Kay, S. M., and Coira, B. L. (2009). "Shallowing and steepening subduction zones, continental lithospheric loss, magmatism, and crustal flow under the Central Andean Altiplano-Puna Plateau," in *Backbone of the americas: Shallow subduction, plateau uplift, and ridge and terrane collision*. Editors S. M. Kay, V. A. Ramos, and W. R. Dickinson (Geological Society of America).

Khin, Z., Meffre, S., Lai, C.-K., Burrett, C., Santosh, M., Graham, I., et al. (2014). Tectonics and metallogeny of mainland Southeast Asia — a review and contribution. *Gondwana Res.* 26 (1), 5–30. doi:10.1016/j.gr.2013.10.010

Lacassin, R., Maluski, H., Leloup, P. H., Tapponnier, P., Hinthong, C., Siribhakdi, K., et al. (1997). Tertiary diachronic extrusion and deformation of western Indochina: structural and $^{40}$Ar/$^{39}$Ar evidence from NW Thailand. *J. Geophys. Research-Solid Earth* 102 (B5), 10013–10037. doi:10.1029/96jb03831

Lee, C., and King, S. D. (2011). Dynamic buckling of subducting slabs reconciles geological and geophysical observations. *Earth Planet. Sci. Lett.* 312 (3), 360–370. doi:10.1016/j.epsl.2011.10.033

Leloup, P. H., and Kienast, J.-R. (1993). High-temperature metamorphism in a major strike-slip shear zone: the Ailao Shan—red River, people's Republic of China. *Earth Planet. Sci. Lett.* 118 (1), 213–234. doi:10.1016/0012-821X(93)90169-A

Leloup, P. H., Lacassin, R., Tapponnier, P., Schärer, U., Dalai, Z., Xiaohan, L., et al. (1995). The Ailao Shan-Red River shear zone (yunnan, China), tertiary transform boundary of Indochina. *Tectonophysics* 251 (1-4), 3–84. doi:10.1016/0040-1951(95)00070-4

Li, J., Cao, S., Neubauer, F., Cheng, X., Wang, H., and Genser, J. (2021). Structure and spatial-temporal relationships of Eocene-Oligocene potassic magmatism linked to the Ailao Shan-Red River shear zone and post-collisional extension. *Lithos* 396-397, 106203. doi:10.1016/j.lithos.2021.106203

Liang, H. Y., Campbell, I. H., Allen, C. M., Sun, W. D., Yu, H. X., Xie, Y. W., et al. (2007). The age of the potassic alkaline igneous rocks along the Ailao Shan–Red River shear zone: implications for the onset age of left-lateral shearing. *J. Geol.* 115 (2), 231–242. doi:10.1086/510801

Lin, Y. L., Yeh, M. W., Lee, T. Y., Chung, S. L., Iizuka, Y., and Charusiri, P. (2013). First evidence of the Cambrian basement in Upper Peninsula of Thailand and its implication for crustal and tectonic evolution of the Sibumasu terrane. *Gondwana Res.* 24 (3), 1031–1037. doi:10.1016/j.gr.2013.05.014

Lin, Y.-L., Lee, T.-Y., Lo, C.-H., Sherlock, S. C., Iizuka, Y., Usuki, T., et al. (2021). Dating deformation using sheared leucogranite: temporal constraints by 40Ar/39Ar thermochronology for the Mae ping shear zone, NW Thailand. *Contrib. Mineral. Petrol.* 176 (9), 65. doi:10.1007/s00410-021-01822-4

Liu, J., Chen, X., Wu, W., Tang, Y., Tran, M.-D., Nguyen, Q.-L., et al. (2015). New tectono-geochronological constraints on timing of shearing along the Ailao Shan-Red River shear zone: implications for genesis of Ailao Shan gold mineralization. *J. Asian Earth Sci.* 103, 70–86. doi:10.1016/j.jseaes.2014.11.006

Ludwig, K. R. (2008). *User's manual for Isoplot 3.70: A geochronological toolkit for microsoft Excel*.

MacDonald, A. S., Barr, S. M., Dunning, G. R., and Yaowanoiyothin, W. (1993). The Doi inthanon metamorphic core complex in NW Thailand: age and tectonic significance. *J. Southeast Asian Earth Sci.* 8 (1), 117–125. doi:10.1016/0743-9547(93)90013-F

Macdonald, A. S., Barr, S. M., Miller, B. V., Reynolds, P. H., Rhodes, B. P., and Yokart, B. (2010). P-T-t constraints on the development of the Doi Inthanon metamorphic core complex domain and implications for the evolution of the western gneiss belt, northern Thailand. *J. Asian Earth Sci.* 37(1), 82–104. DOI doi:10.1016/j.jseaes.2009.07.010

Mako, C. A., and Caddick, M. J. (2018). Quantifying magnitudes of shear heating in metamorphic systems. *Tectonophysics* 744, 499–517. doi:10.1016/j.tecto.2018.07.003

Metcalfe, I. (2011). Tectonic framework and phanerozoic evolution of sundaland. *Gondwana Res.* 19(1), 3–21. doi:10.1016/j.gr.2010.02.016

Metcalfe, I. (2013). Gondwana dispersion and asian accretion: tectonic and palaeogeographic evolution of eastern Tethys. *J. Asian Earth Sci.* 66, 1–33. doi:10.1016/j.jseaes.2012.12.020

Mezger, K., and Krogstad, E. J. (1997). Interpretation of discordant U-Pb zircon ages: an evaluation. *J. Metamorph. Geol.* 15 (1), 127–140. doi:10.1111/j.1525-1314.1997.00008.x

Mickein, A. (1997). U/Pb-, Rb/Sr-und K/Ar-Untersuchungen zur metamorphen Entwicklung und Alterstellung des "Präkambriums" in NW-Thailand. *Gött. Arb. Zur Geol. Paläontol.* 73, 1–83.

Morley, C. K., Smith, M., Carter, A., Charusiri, P., and Chantraprasert, S. (2007). Evolution of deformation styles at a major restraining bend, constraints from cooling histories, Mae Ping fault zone, western Thailand. *Geol. Soc. Lond. Spec. Publ.* 290, 325–349. doi:10.1144/SP290.12

Nantasin, P., Hauzenberger, C., Liu, X., Krenn, K., Dong, Y., Thöni, M., et al. (2012). Occurrence of the high grade thabsila metamorphic complex within the low grade three Pagodas shear zone, kanchanaburi province, western Thailand: petrology and geochronology. *J. Asian Earth Sci.* 60 (0), 68–87. doi:10.1016/j.jseaes.2012.07.025

Neves, S. P., Vauchez, A., and Archanjo, C. J. (1996). Shear zone-controlled magma emplacement or magma-assisted nucleation of shear zones? Insights from northeast Brazil. *Tectonophysics* 262 (1), 349–364. doi:10.1016/0040-1951(96)00007-8

Österle, J. E., Klötzli, U., Stockli, D. F., Palzer-Khomenko, M., and Kanjanapayont, P. (2019). New age constraints on the Lan Sang gneiss complex, Thailand, and the timing of activity of the Mae Ping shear zone from *in-situ* and depth-profile zircon and monazite U-Th-Pb geochronology. *J. Asian Earth Sci.* 181, 103886. doi:10.1016/j.jseaes.2019.103886

Palin, R. M., Searle, M. P., Morley, C. K., Charusiri, P., Horstwood, M. S. A., and Roberts, N. M. W. (2013). Timing of metamorphism of the Lansang gneiss and implications for left-lateral motion along the Mae Ping (Wang Chao) strike-slip fault, Thailand. *J. Asian Earth Sci.* 76, 120–136. doi:10.1016/j.jseaes.2013.01.021

Passchier, C. W., and Trouw, R. A. J. (2005). *Microtectonics*. Springer.

Peltzer, G., and Tapponnier, P. (1988). Formation and evolution of strike-slip faults, rifts, and basins during the India-Asia collision: an experimental approach. *J. Geophys. Res. Solid Earth* 93 (B12), 15085–15117. doi:10.1029/JB093iB12p15085

Pitcher, W. S., and Bussell, M. A. (1977). Structural control of batholithic emplacement in Peru: a review. *J. Geol. Soc.* 133 (3), 249–255. doi:10.1144/gsjgs.133.3.0249

Polachan, S., Pradidtan, S., Tongtaow, C., Janmaha, S., Intarawijitr, K., and Sangsuwan, C. (1991). Development of cenozoic basins in Thailand. *Mar. Petrol. Geol.* 8 (1), 84–97. doi:10.1016/0264-8172(91)90047-5

Reddy, S. M., and Potts, G. J. (1999). Constraining absolute deformation ages: the relationship between deformation mechanisms and isotope systematics. *J. Struct. Geol.* 21 (8-9), 1255–1265. doi:10.1016/S0191-8141(99)00032-2

Rosenberg, C. L., and Handy, M. R. (2005). Experimental deformation of partially melted granite revisited: implications for the continental crust. *J. Metamorph. Geol.* 23 (1), 19–28. doi:10.1111/j.1525-1314.2005.00555.x

Rosenberg, C. L. (2004). Shear zones and magma ascent: A model based on a review of the tertiary magmatism in the alps. *Tectonics* 23 (3). doi:10.1029/2003TC001526

Rubatto, D. (2002). Zircon trace element geochemistry: partitioning with garnet and the link between U-Pb ages and metamorphism. *Chem. Geol.* 184 (1-2), 123–138. doi:10.1016/s0009-2541(01)00355-2

Rubatto, D. (2017). Zircon: the metamorphic mineral. *Rev. Mineral. Geochem.* 83 (1), 261–295. doi:10.2138/rmg.2017.83.9

Schaltegger, U., Fanning, C. M., Günther, D., Maurin, J. C., Schulmann, K., and Gebauer, D. (1999). Growth, annealing and recrystallization of zircon and preservation of monazite in high-grade metamorphism: conventional and *in-situ* U-Pb isotope, cathodoluminescence and microchemical evidence. *Contributions Mineralogy Petrology* 134 (2), 186–201. doi:10.1007/s004100050478

Scharer, U., Zhang, L. S., and Tapponnier, P. (1994). Duration of strike-slip movements in large shear zones - the Red River belt, China. *Earth Planet. Sci. Lett.* 126 (4), 379–397. doi:10.1016/0012-821x(94)90119-8

Searle, M. P., Whitehouse, M. J., Robb, L. J., Ghani, A. A., Hutchison, C. S., Sone, M., et al. (2012). Tectonic evolution of the sibumasu-indochina terrane collision zone in Thailand and Malaysia: constraints from new U-Pb zircon chronology of SE asian tin granitoids. *J. Geol. Soc.* 169 (4), 489–500. doi:10.1144/0016-76492011-107

Searle, M. P. (2006). Role of the Red River shear zone, yunnan and vietnam, in the continental extrusion of SE Asia. *J. Geol. Soc.* 163 (6), 1025–1036. doi:10.1144/0016-76492005-144

Sone, M., Metcalfe, I., and Chaodumrong, P. (2012). The chanthaburi terrane of southeastern Thailand: stratigraphic confirmation as a disrupted segment of the Sukhothai arc. *J. Asian Earth Sci.* 61, 16–32. doi:10.1016/j.jseaes.2012.08.021

Stipp, M., Stünitz, H., Heilbronner, R., and Schmid, S. M. (2002). The eastern tonale fault zone: a 'natural laboratory' for crystal plastic deformation of quartz over a temperature range from 250 to 700 °C. *J. Struct. Geol.* 24 (12), 1861–1884. doi:10.1016/S0191-8141(02)00035-4

Strong, D. F., and Hanmer, S. K. (1981). The leucogranites of southern Brittany; origin by faulting, frictional heating, fluid flux and fractional melting. *Can. Mineralogist* 19 (1), 163–176.

Tang, Y., Liu, J., Tran, M.-D., Song, Z., Wu, W., Zhang, Z., et al. (2013). Timing of left-lateral shearing along the Ailao Shan-Red River shear zone: constraints from zircon U–Pb ages from granitic rocks in the shear zone along the Ailao Shan range, western yunnan, China. *Int. J. Earth Sci.* 102 (3), 605–626. doi:10.1007/s00531-012-0831-y

Tapponnier, P., Peltzer, G., Ledain, A. Y., Armijo, R., and Cobbold, P. (1982). Propagating extrusion tectonics in Asia - new insights from simple experiments with plasticine. *Geology* 10 (12), 611–616. doi:10.1130/0091-7613(1982)10<611:petian>2.0.co;2

Teggin, D. E. (1975). *The granites of northern Thailand*. Ph.D., Manchester University.

Tommasi, A., Vauchez, A., Femandes, L. A. D., and Porcher, C. C. (1994). Magma-assisted strain localization in an orogen-parallel transcurrent shear zone of southern Brazil. *Tectonics* 13 (2), 421–437. doi:10.1029/93TC03319

Uchida, E., Nagano, S., Niki, S., Yonezu, K., Saitoh, Y., Shin, K.-C., et al. (2022). Geochemical and radiogenic isotopic signatures of granitic rocks in chanthaburi and chachoengsao provinces, southeastern Thailand: implications for origin and evolution. *J. Asian Earth Sci. X* 8, 100111. doi:10.1016/j.jaesx.2022.100111

Ueno, K., and Hisada, K.-i. (2001). The nan-uttaradit-sa kaeo suture as a main paleo-tethyan suture in Thailand: is it real? *Gondwana Res.* 4 (4), 804–806. doi:10.1016/S1342-937X(05)70590-6

Veeravinantanakul, A., Takahashi, R., Agangi, A., Ohba, T., Watanabe, Y., Elburg, M. A., et al. (2021). Zircon Hf-isotope constraints on the formation of metallic mineral deposits in Thailand. *Resour. Geol.* 71 (4), 436–469. doi:10.1111/rge.12276

Wang, P.-L., Lo, C.-H., Lee, T.-Y., Chung, S.-L., Lan, C.-Y., and Yem, N. T. (1998). Thermochronological evidence for the movement of the Ailao Shan–Red River shear zone: A perspective from vietnam. *Geology* 26 (10), 887–890. doi:10.1130/0091-7613(1998)026<0887:Teftmo>2.3.Co;2

Wang, S., Mo, Y., Wang, C., and Ye, P. (2016). Paleotethyan evolution of the Indochina Block as deduced from granites in northern Laos. *Gondwana Res.* 38, 183–196. doi:10.1016/j.gr.2015.11.011

Watkinson, I., Elders, C., Batt, G., Jourdan, F., Hall, R., and McNaughton, N. J. (2011). The timing of strike-slip shear along the Ranong and Khlong Marui faults, Thailand. *J. Geophys. Res. Solid Earth* 116 (B9), B09403. doi:10.1029/2011jb008379

West, D. P., and Lux, D. R. (1993). Dating mylonitic deformation by the 40Ar-39Ar method: an example from the norumbega fault zone, Maine. *Earth Planet. Sci. Lett.* 120 (3), 221–237. doi:10.1016/0012-821X(93)90241-Z

Whitney, D. L., and Evans, B. W. (2010). Abbreviations for names of rock-forming minerals. *Am. Mineral.* 95 (1), 185–187. doi:10.2138/am.2010.3371

Yakymchuk, C., Kirkland, C. L., and Clark, C. (2018). Th/U ratios in metamorphic zircon. *J. Metamorph. Geol.* 36 (6), 715–737. doi:10.1111/jmg.12307

Zhang, L.-S., and Schärer, U. (1999). Age and origin of magmatism along the Cenozoic Red River shear belt, China. *Contributions Mineralogy Petrology* 134 (1), 67–85. doi:10.1007/s004100050469

Zhang, X., Chung, S. L., Lai, Y. M., Ghani, A. A., Murtadha, S., Lee, H. Y., et al. (2019). A 6000-km-long Neo-Tethyan arc system with coherent magmatic flare-ups and lulls in South Asia. *Geology* 47 (6), 573–576. doi:10.1130/g46172.1